The Company of **Biologists**

RESEARCH ARTICLE

Glypican 4 and Mmp14 interact in regulating the migration of anterior endodermal cells by limiting extracellular matrix deposition

Bo Hu[1], Yuanyuan Gao[1], Lauren Davies[1], Stephanie Woo[2], Jacek Topczewski[3,4], Jason R. Jessen[5] and Fang Lin[1,*]

ABSTRACT

During embryogenesis, the germ layers, including the endoderm, undergo convergence and extension movements to narrow and elongate the body plan. In zebrafish, the dorsal migration of endodermal cells during gastrulation is controlled by chemokine signaling, but little is known about how they migrate during segmentation. Here, we show that glypican 4 (Gpc4), a member of the heparin sulfate proteoglycan family, is required for efficient migration of anterior endodermal cells during early segmentation, regulating Rac activation to maintain polarized actin-rich lamellipodia. An endoderm transplantation assay showed that Gpc4 regulates endoderm migration in a non-cell-autonomous fashion. Further analyses revealed that the impaired endoderm migration in *gpc4* mutants results from increases in the expression and assembly of fibronectin and laminin, major components of the extracellular matrix (ECM). Notably, we found that matrix metalloproteinase 14 (Mmp14a/b) is required for the control of ECM expression during endoderm migration, with Gpc4 acting through Mmp14a/b to limit ECM expression. Our results suggest that Gpc4 is crucial for generating the environment required for efficient migration of endodermal cells, uncovering a novel function of Gpc4 during development.

KEY WORDS: Glypican 4, Endoderm, Cell migration, Imaging, Extracellular matrix

INTRODUCTION

The endoderm, the deepest germ layer, contributes to the development of the digestive system, heart and craniofacial structures. During embryogenesis, three germ layers (ectoderm, mesoderm and endoderm) form and undergo coordinated morphogenetic movements, including convergence and extension (CE): a process that narrows and elongates the germ layers to establish the animal body plan (Keller, 2002; Montero and Heisenberg, 2004; Solnica-Krezel and Sepich, 2012). During zebrafish gastrulation, the migratory behavior and regulatory

mechanisms that drive CE in the mesoderm and endoderm are distinct. Cells in the mesoderm exhibit progressive mediolateral polarization, directed dorsal migration and mediolateral intercalation, processes that are largely controlled by non-canonical Wnt/planar cell polarity (Wnt/PCP) pathway (Keller, 2002; Solnica-Krezel and Sepich, 2012). In many species, deficiency for PCP proteins (including Wnt5, Wnt11, Fzd7 and Vangl2) results in the production of embryos with shorter, broader body axes because mesodermal cells fail to polarize and migrate efficiently (Roszko et al., 2009). Additionally, in both *Xenopus* and zebrafish, glypican 4 (Gpc4), a member of the heparan sulfate proteoglycan (HSPGs) family, is required for CE, likely acting as a co-receptor with Fzd for Wnt to promote Wnt11 function (Ohkawara et al., 2003; Topczewski et al., 2001).

Endodermal cells exhibit different migratory behaviors at distinct stages of gastrulation. Initially, endodermal cells are large, flat and have numerous filopodia (Warga and Nüsslein-Volhard, 1999). They engage in non-directed movement, a so-called 'random walk', to disperse over the yolk, which is regulated by TGF/Nodal signaling (Pézeron et al., 2008; Woo et al., 2012). After mid-gastrulation, endodermal migration resembles its mesodermal counterpart, with individual cells migrating towards the dorsal side of the embryo under the control of Cxcl12b-Cxcr4a chemokine signaling (Mizoguchi et al., 2008; Nair and Schilling, 2008). Notably, such chemokine signaling is not required for migration of the mesoderm (Mizoguchi et al., 2008), but instead regulates integrin-mediated adhesion between the endoderm and mesoderm (Nair and Schilling, 2008). These data suggest that the migration of endodermal and mesodermal cells during gastrulation is regulated by different signaling pathways.

During segmentation, the point at which somites begin to develop, endodermal cells continue CE movements. The cells in the anterior region contribute to formation of the endodermal pouches (Ye et al., 2015): structures that are key to craniofacial development (Choe and Crump, 2015), whereas the cells in the posterior region contribute to formation of the gut and the associated organs (Miles et al., 2017; Ober et al., 2003). We have previously shown that after mid-segmentation (from 6-8s), endodermal cells in the anterior region form cell-cell contacts and migrate collectively, as a cohesive sheet, under the regulation of a sphingosine-1-phosphate G-protein-coupled receptor, S1pr2, and its cognate G protein isoform, Gα_{13} (Ye and Lin, 2013; Ye et al., 2015). Endoderm morphogenesis also seems to involve Wnt/PCP signaling. In zebrafish, injection of multiple morpholinos (MOs) targeting *wnt4a*, *wnt11* and *wnt11r* disrupts the medial migration of both mesodermal and endodermal cells in the anterior region (Matsui et al., 2005), and Vangl2 and Gpc4 are involved in morphogenesis of the posterior endoderm (Miles et al., 2017). In the case of mice,

[1]Department of Anatomy and Cell Biology, Carver College of Medicine, University of Iowa, Iowa City, IA 52242, USA. [2]School of Natural Sciences, Merced, University of California Merced, Merced, CA 95340, USA. [3]Northwestern University, Feinberg School of Medicine, Stanley Manne Children's Research Institute, Chicago, IL 60611, USA. [4]Department of Biochemistry and Molecular Biology, Medical University of Lublin, Lublin 20-093, Poland. [5]Department of Biology, Middle Tennessee State University, Murfreesboro, TN 37132, USA.

*Author for correspondence (fang-lin@uiowa.edu)

F.L., 0000-0002-1972-9294

DEVELOPMENT

1

PCP signaling is involved in migration of the visceral endoderm (Trichas et al., 2012). Notwithstanding these findings, how Wnt/PCP signaling regulates endoderm morphogenesis during segmentation is poorly understood.

Here, we report that Gpc4 is required for the migration of anterior endodermal cells throughout segmentation. We focus on early segmentation, from the tailbud stage (TB) to the six-somite stage (6s), when endodermal cells migrate as individual cells. Our studies reveal that Gpc4 is required for efficient endodermal migration, at least by regulating the spatial activation of Rac1. Furthermore, transplantation analysis shows that Gpc4 modulates endoderm migration in a non-cell-autonomous manner, likely by regulating assembly of the extracellular matrix (ECM) surrounding endodermal cells. Thus, our studies reveal that Gpc4 is crucial for generating an environment needed for efficient migration of endodermal cells. This represents a new role of Gpc4 in endoderm morphogenesis.

RESULTS
Gpc4 is required for convergent movement of the anterior endoderm

To explore the role of Wnt/PCP signaling in endoderm morphogenesis, we examined the expression of *gpc4* and *vangl2*, components of the Wnt/PCP signaling pathway. Using fluorescence-activated cell sorting (FACS), endodermal cells were isolated from 18s *Tg(sox17:EGFP)* embryos, in which the endoderm is labeled with EGFP. RT-PCR analysis of the sorted cells revealed that both *gpc4* and *vangl2* are expressed in the endoderm, and that *vangl1* is also expressed, although at much lower levels (Fig. S1A). Expression of *gpc4* and *vangl2* was confirmed by *in situ* hybridization; both genes were expressed ubiquitously (including in the endoderm) at 80% epiboly (mid-gastrulation) and at 10s (Fig. S1B-I″).

To examine endoderm morphology in the absence of *gpc4* and *vangl2,* we performed *in situ* hybridization for *foxa2* on 22s *knypek*[fr6] and *trilobite*[uv67] mutants, which harbor non-functional *gpc4* and *vangl2* genes and will subsequently be referred to as *gpc4* and *vangl2* mutants, respectively (Jessen et al., 2002; Topczewski et al., 2001). We found that *foxa2* was expressed normally in both mutant embryos; however, the endodermal sheet was wider in only the *gpc4* mutant embryos, although the body axes were shorter in both mutants, as previously reported (Fig. S2A-C′) (Jessen et al., 2002; Topczewski et al., 2001). Quantification using *Tg(sox17:H2A-mCherry)* embryos confirmed that the endodermal sheet was significantly wider in *gpc4* mutants than that in siblings (Fig. S3A-B,E). Notably, when an RNA encoding *GFP-gpc4* was injected into *gpc4* mutant embryos, the length of the body axis was largely restored (Fig. S3F-I) and defects in endodermal width were completely rescued (Fig. S3B-E). These findings indicate that the loss of Gpc4 is responsible for endodermal defects, and Gpc4 is required for the migration, but not specification, of endodermal cells. We also assessed endodermal morphogenesis at earlier stages: at the end of gastrulation (TB), by performing *in situ* hybridization for *sox17*; and at early-segmentation (6s), using *Tg(sox17:EGFP)* embryos. We found that *sox17* was expressed normally in both *vangl2* and *gpc4* mutant embryos, but that endoderm morphology was abnormal specifically in the *gpc4* mutants (Fig. S2D-F). At TB, the point at which gastrulation is complete, endodermal cells in both control and *vangl2* mutant embryos had migrated towards the dorsal site of the embryo; however, the distance between the lateral-most endodermal cells and the dorsal site of embryo in *gpc4* mutant embryos was greater than that in control siblings (Fig. S2D-F).

During segmentation, endodermal cells in control embryos continue CE movements. Whereas in *vangl2* mutants the width of the anterior endoderm did not differ significantly from that in control siblings (Fig. S2G-I), in the case of *gpc4* mutants it continued to become wider (Fig. 1B,B′). These data indicate that endoderm migration depends on Gpc4, but not Vangl2, from the end of gastrulation through segmentation.

Gpc4 is required for efficient CE movements of the anterior endodermal cells

To identify cellular behaviors that contribute to CE movements of the anterior endodermal cells during early segmentation and to determine the role that Gpc4 plays in this process, we performed time-lapse experiments on *Tg(sox17:EGFP)* embryos from TB to 6s (Movie 1). Cell-tracking analyses revealed that endodermal cells migrate individually during this period, in both the medial and anterior directions, to narrow and extend (in the anteroposterior direction) the endodermal sheet (Fig. 1A,A′). Two patterns of migration were observed in distinct cell populations: primarily anterior migration of cells located near the notochord (blue tracks), contributing to extension of the endoderm along the anteroposterior axis; and medial migration (toward the midline) of more laterally located cells (magenta tracks), contributing to convergence of the endoderm along the lateral axis (Fig. 1C). In *gpc4* mutant embryos, these two populations of endodermal cells migrated in the anterior and medial directions, respectively, i.e. they retained their overall migration patterns (Fig. 1D). However, they migrated in more circuitous paths than their control counterparts (Fig. 1C-D), suggesting that Gpc4 is required for efficient migration of these cells.

We next analyzed the two cell populations that engaged in medial migration (convergence) and anterior migration (extension) separately. We first assessed total convergence and extension speeds, i.e. for movements in all directions, and found that in *gpc4* mutants both populations migrated at a similar speed as in the control embryos (Fig. 1E). Thus, the general motility of *gpc4* mutant endodermal cells was not affected. However, the net convergence and extension speeds, i.e. for only those movements that account for the actual CE, were strongly compromised in mutant cells (Fig. 1E). Additionally, the migration persistence index (defined as the ratio of net:total distance traveled) for convergence and extension was also lower in mutants (Fig. 1F). Thus, in the absence of *gpc4*, endodermal cells migrate less efficiently during endoderm CE.

Analysis of the direction of all cell movement events throughout the time-lapse period (5 min intervals) was undertaken (Fig. 1G). In the case of cells engaged in convergence (left panel), in controls 62% out of 928 events were in the medial direction (between +60° and −30° of the mediolateral axis) and only 13% were in the opposite direction (within −90° to −150° of the mediolateral axis); in the *gpc4* mutants, by contrast, 40% out of 957 total events were in the medial direction and 33% were in the opposite direction. Similarly, for cells engaged in extension (Fig. 1G, right panel), in controls 51% out of 491 events were in the anterior direction (within ±30° of the anterior-posterior axis) and 18% were in the posterior direction (within ±150° of the anterior-posterior axis); in *gpc4* mutant embryos, 42% out of 464 events were in the anterior direction and 30% were in the posterior direction. These data indicate that *gpc4* mutant endodermal cells fail to migrate in the correct direction, and that this is the cause of the impairment in endoderm CE. Together, these analyses reveal that Gpc4 function is
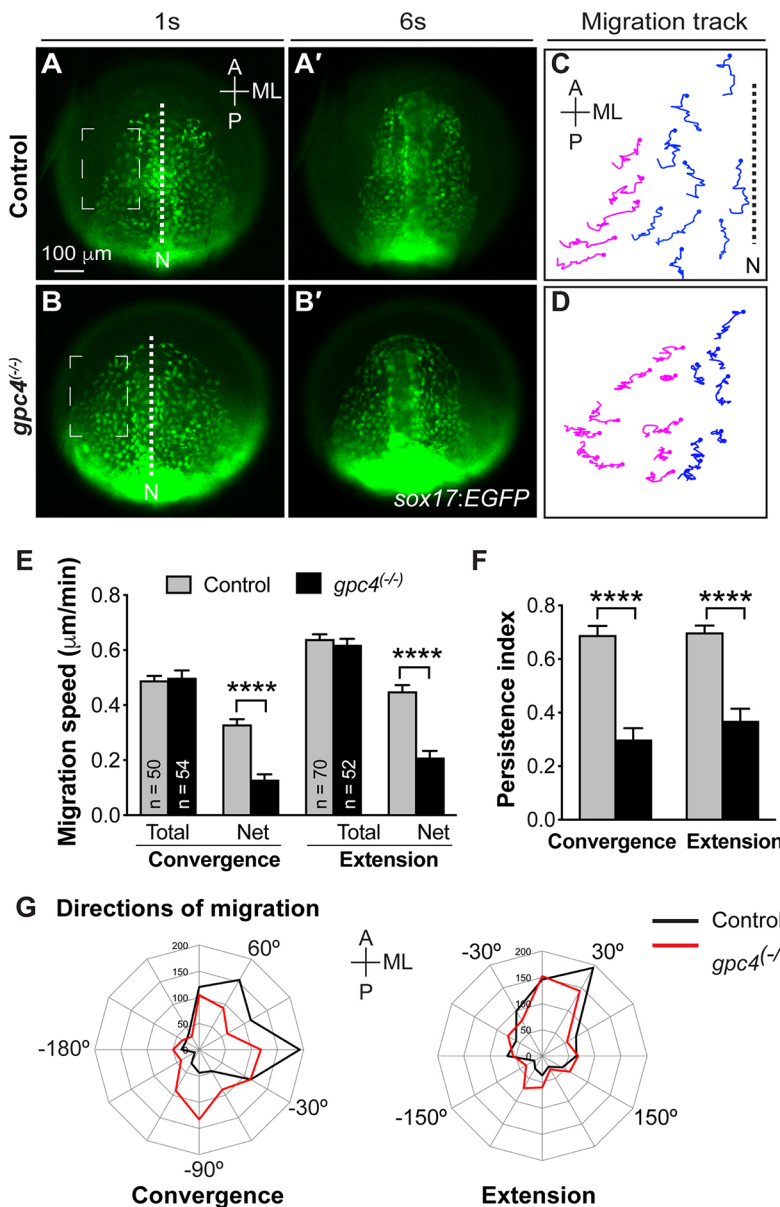
Fig. 1. Glypican 4 is required for efficient convergence and extension movements of cells of the anterior endoderm during early segmentation. Epifluorescence time-lapse experiments performed on the anterior endoderm of one- to six-somite stage (s) *Tg(sox17:EGFP)* embryos (Movie 1). (A-B′) Representative still images from movies at 1s (A,B) and 6s (A′,B′). Dashed squares indicate locations in which cell migration was analyzed. (C,D) Representative migration tracks of two populations of endodermal cells detected in A and in B. Blue and magenta tracks represent cells that migrate primarily in the anterior and medial directions, respectively. Solid circles indicate the endpoint of migration. N, notochord. (E-G) Characteristics of migration. Six embryos of each genotype were analyzed, and the number of cells analyzed for each genotype is indicated in the graph. (E) Total and net speeds of convergence and extension. (F) Persistence index for migration. ****$P<0.0001$; Student's *t*-test. (G) Direction of cell migration during the time-lapse period (5 min intervals, grouped into 30° sectors). A, anterior; P, posterior; ML, medial-lateral.

required for effective directed migration of anterior endodermal cells during early segmentation.

Gpc4 is required for maintaining actin-rich protrusions in the leading edge of migrating endodermal cells

During late gastrulation, endodermal cells in the lateral region undergo persistent medial migration, powered by persistent actin-based lamellipodia in the leading edge of the cell (Woo et al., 2012). To investigate how Gpc4 regulates the migratory behaviors of endodermal cells, we performed confocal time-lapse imaging, monitoring dynamics of the actomyosin cytoskeleton using the transgenic line *Tg(sox17:GFP-UTRN)*, in which the endodermal F-actin-binding domain of utrophin (UTRN) is tagged with GFP (Burkel et al., 2007; Woo et al., 2012). We found that at TB, cells in the dorsal-anterior region underwent a migration process similar to that of the lateral cells during gastrulation, becoming polarized and preferentially extending actin-rich broad lamellipodia mainly in the direction of migration (Fig. 2A-D, Movie 2). Notably, these lamellipodia-like protrusions persisted for as long as 4 min

(Fig. 2J); this is much longer than that reported for lateral endodermal cells (1.5 min) (Woo et al., 2012). In *gpc4* mutant embryos, endodermal cells appeared to be elongated but failed to develop a single broad lamellipodium, instead simultaneously forming multiple smaller actin-rich protrusions around their perimeter (Fig. 2E-H, Movie 2). Analysis of protrusions revealed that those in control cells extended mainly from the leading edge of cells (44%), with some extending from the trailing and lateral edges (27% and 30%); in mutant cells much fewer protrusions extended from the leading edge (27%) and more extended from the lateral edges (48%) (Fig. 2I). Additionally, we found that compared with sibling control counterparts, *gpc4* mutant endodermal cells have more total number of protrusions (per minute per cell, 12.3 versus 7.3) and formed many more new protrusions (over 1 min per cell, 4 vs 2.5) (Fig. 2J). Additionally, the protrusions in *gpc4* mutant cells were significantly shorter lived, lasting only 2.5 min (Fig. 2J). These unstable and multi-directional cell protrusions likely account for the inefficient migration of endodermal cells in *gpc4* mutants.
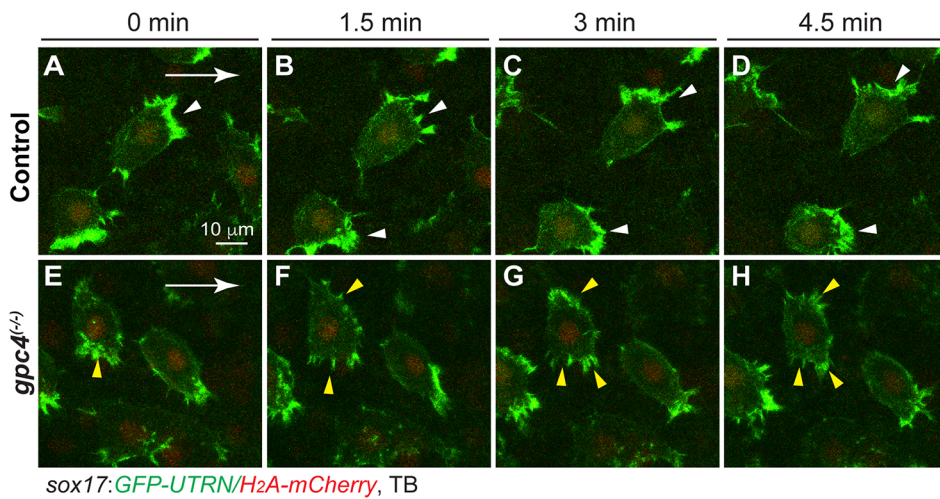
Fig. 2. Glypican 4 is required to maintain polarized actin-rich protrusions on migrating endodermal cells. Actin dynamics were assessed by tracking endodermal cells expressing GFP-UTRN (Movie 2). (A-H) Snapshots from confocal time-lapse imaging at different time points. Broader lamellipodia are marked by white arrowheads (control cells) and smaller lamellipodia by yellow arrowheads (*gpc4* mutant cells). White arrows indicate the direction of migration of endodermal cells. (I) Direction of protrusions relative to the direction of cell migration in sibling and *gpc4* mutant embryos (2 min intervals, grouped into 30° sectors). Percentage of protrusions in various directions (leading, ±30°; trailing, ±150°; lateral, ±30-150°) is shown. (J) Average total protrusions (in each endodermal cell, as assessed at 1 min intervals throughout the imaging period, 1286 protrusions in 11 control cells, 1091 protrusions in eight mutant cells), newly formed protrusions (in each endodermal cell per minute, 443 protrusions in 11 control cells, 326 protrusions in six mutant cells) and the duration of protrusions in control (50 protrusions, 11 cells) and *gpc4* mutants (31 protrusions, eight cells). ****$P<0.0001$; Student's *t*-test.
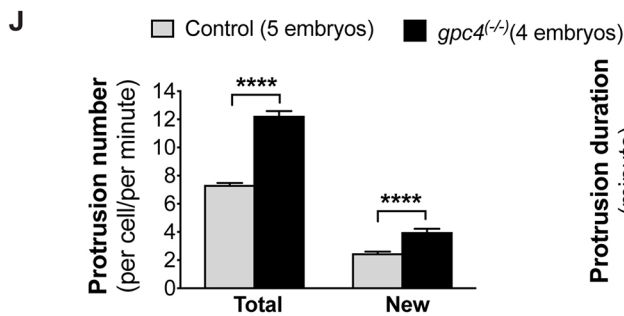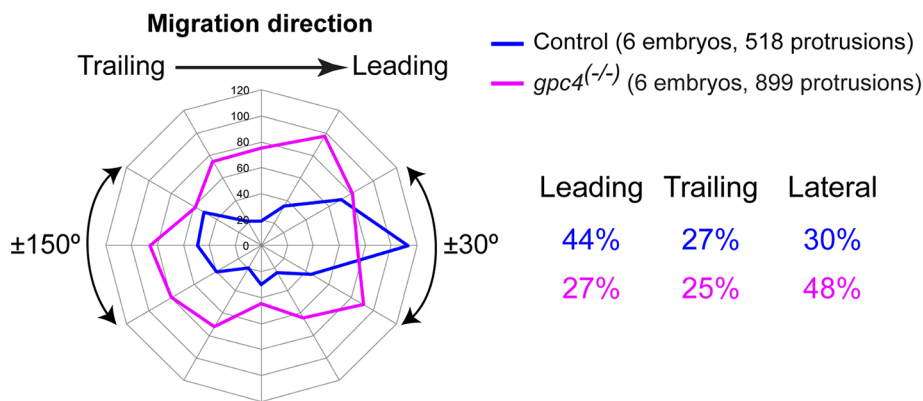
During gastrulation, the directional lamellipodia of endodermal cells is controlled by Rac1 activation (Woo et al., 2012). Therefore, we next determined whether Gpc4 influences the migration of endodermal cells by regulating Rac1 activity. We monitored Rac1 activation in endodermal cells *in vivo* using a GFP-PBD probe, in which the Rac1-binding domain of p21-activated kinase is fused with GFP and binds to active GTP-bound Rac (Miller and Bement, 2009; Srinivasan et al., 2003). To facilitate image analysis, we labeled subpopulations of endodermal cells by endoderm transplantation, as described previously (Kardash et al., 2011; Woo et al., 2012) (Fig. 3A). Confocal time-lapse microscopy was performed on the dorsal anterior endodermal cells at TB, and Rac activity was determined as the ratio of the GFP:dextran signals (Woo et al., 2012). We found that active Rac1 signal was enriched in the leading protrusions (Fig. 3B), consistent with the findings in lateral endodermal cells at mid-gastrulation (Woo et al., 2012). In *gpc4* mutant embryos, Rac1 activation in endodermal cells was not

polarized and overall Rac activity was lower than in control cells (Fig. 3C,D, Movie 3). Thus, reduced Rac activation in *gpc4*-deficient endodermal cells likely impairs actin dynamics and protrusive activity in the leading edge of these cells, thereby disrupting cell migration during endoderm CE. Collectively, these results suggest that Gpc4 promotes Rac1 activation at the leading region of endodermal cells to regulate actin dynamics during the CE movements of these cells.

Gpc4 regulates the migration of endodermal cells in a non-cell-autonomous fashion

HSPGs bind to the external surface of the plasma membrane. They do not directly trigger cellular processes but rather regulate signaling mediated by various morphogens, including Wnt, by either acting as co-receptors or controlling morphogen diffusion/trafficking (Fico et al., 2011; Filmus et al., 2008; Poulain and Yost, 2015; Song and Filmus, 2002). In zebrafish and *Xenopus*, Gpc4 is
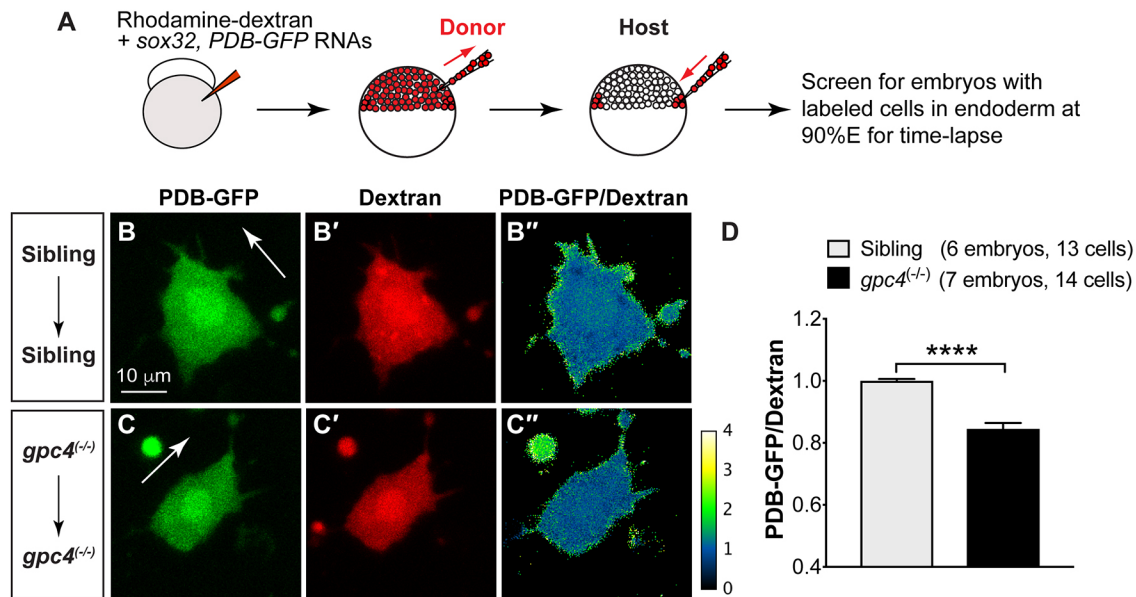
Fig. 3. Glypican 4 regulates Rac1 activity in migratory endodermal cells. (A) Schematic diagram illustrating the endoderm transplantation procedure. Donor embryos obtained from crossing *gpc4* heterozygous fish were injected with *sox32* and *PDB-GFP* RNAs plus rhodamine-dextran (a marker of cell volume) at the one-cell stage. At the blastula stage, 30-50 donor cells were transplanted into host embryos obtained from crossing *gpc4* heterozygous fish. (B-C″) Confocal time-lapse analysis of endodermal cells expressing (B,C) PDB-GFP, a fluorescent Rac1 probe, and (B′,C′) dextran. Rac activity was determined as the ratio of the PDB-GFP:dextran signals, and is displayed as radiometric pseudocolored images (B″,C″). Yellow indicates a higher value of PBD relative to dextran. White arrows indicate the direction of migration of endodermal cells (Movie 3). (D) The mean ratio of PDB-GFP:dextran in indicated embryos. The numbers of embryos and cells analyzed are shown. ****$P<0.0001$; Student's *t*-test.

known to regulate mesoderm CE by modulating Wnt/PCP signaling (Ohkawara et al., 2003; Topczewski et al., 2001). However, our data showed that endoderm morphology is normal in mutants for *vangl2*, a PCP core gene, at both gastrulation and segmentation (Fig. S2). Given that cell polarity within the plane is a hallmark of PCP (Butler and Wallingford, 2017; Gray et al., 2011) and planar polarity of mesodermal cells is impaired in both *gpc4* and *vangl2* mutants at gastrulation (Jessen et al., 2002; Topczewski et al., 2001), we further assessed the morphology of anterior endodermal cells in *gpc4* mutants at 4s. In the anterior endodermal sheet of control embryos, we observed two populations of endodermal cells based on differences in cell morphology: outer cells near the lateral-most region that were elongated [length-width ratio (LWR), 2.0±0.11]; and inner cells that were more round (LWR, 1.6±0.04) (Fig. S4A,B,E). Thus, endodermal cells do not exhibit uniform planar cell polarity. In *gpc4* mutants, two populations of endodermal cells were also observed and their LWRs were similar to those of control embryos (Fig. S4C-E). Taken together, these data indicate that Wnt/PCP signaling is not involved in the migration of anterior endodermal cells and that Gpc4 is not required for endodermal cell polarity at this stage.

Our results indicate that Gpc4 is required for endoderm migration from late gastrulation through segmentation (Figs 1,2, Figs S2,S3), when it is needed for CE of mesodermal cells (Topczewski et al., 2001). Given our RT-PCR and *in situ* hybridization findings showing that *gpc4* is expressed in both mesoderm and endoderm (Fig. S1), Gpc4 could function within either or both tissues to regulate endoderm migration. To determine which is the case, we performed an endoderm transplantation experiment. To assess the ability of *gpc4* mutant endodermal cells to migrate in a wild-type environment, we transplanted cells from embryos derived from crosses among *gpc4* heterozygous fish into wild-type *Tg(sox17:EGFP)* hosts. To evaluate how wild-type cells migrate in a *gpc4* mutant environment, we performed the

converse experiment, transplanting wild-type donor cells into host embryos derived from crossing heterozygous *gpc4*/*Tg(sox17: EGFP)* fish. Host embryos in which rhodamine-labeled donor endodermal cells were transplanted into one side of the anterior endoderm were selected for time-lapse experiments (Fig. 4, Movies 4 and 5).

In wild-type host embryos, we observed similar patterns of migration between the host and *gpc4* mutant donor endoderm cells (Fig. 4A,A′, Movie 4). Analyses of cell migration revealed similar migratory tracks and speeds for the *gpc4* mutant and wild-type host endodermal cells (Fig. 4B,C,G). Strikingly, in host embryos deficient for *gpc4*, wild-type donor cells did not migrate normally, displaying migration behaviors (circuitous migratory paths and reduced net velocity) similar to those of mutant endodermal cells (Fig. 4D-F,H, Movie 4). These data suggest that the host environment influences the migration of donor endodermal cells, and that Gpc4 regulates endoderm migration in a non-cell-autonomous manner.

Gpc4 modulates endoderm CE by limiting the assembly of fibronectin and laminin

In *gpc4* mutants, the assembly of fibronectin (Fn), a component of the extracellular matrix, is increased during gastrulation (Dohn et al., 2013), suggesting that Gpc4 can influence ECM assembly. Endodermal migration during gastrulation requires integrin-dependent adhesion between these cells and the ECM (Nair and Schilling, 2008). Thus, we postulate that Gpc4 affects the migration of anterior endodermal cells during segmentation by influencing ECM assembly. To test this, we performed immunostaining for Fn and laminin (Lam) on cross-sections of *Tg(sox17:GFP)* embryos at TB and 4s. Using the GFP-expressing endodermal layer as a landmark, we found that in the anterior region of embryos at TB, Fn fibrils were enriched between the ectoderm/mesoderm (ect/mes) boundary, as well as around the GFP-expressing endodermal region
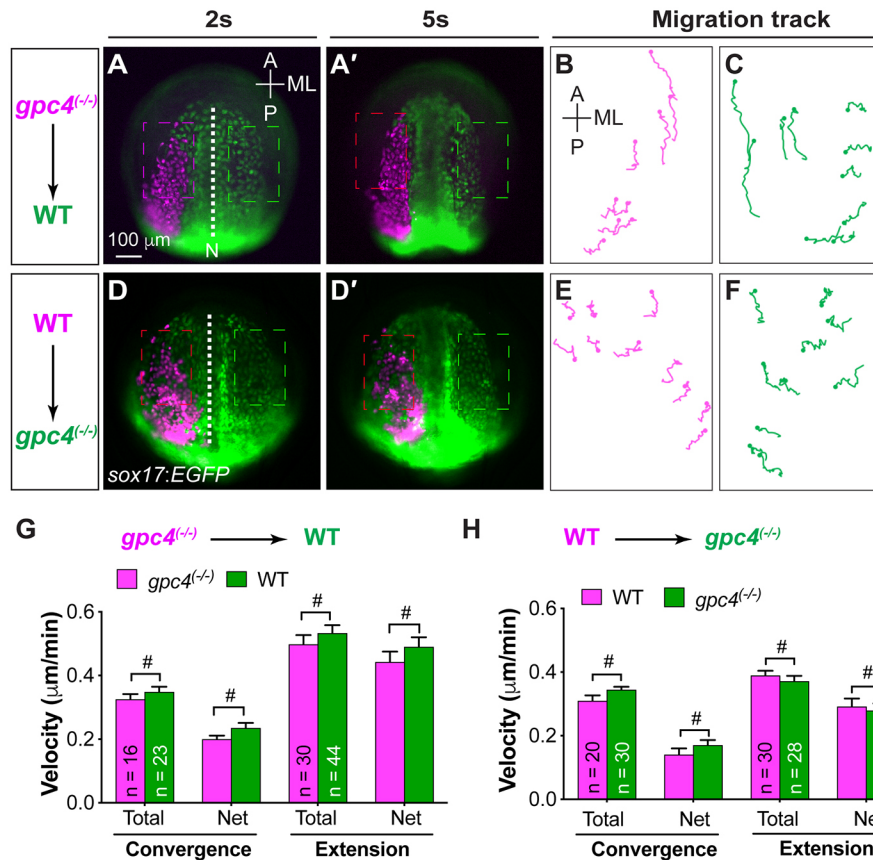
Fig. 4. Glypican 4 regulates endodermal migration in a non-cell-autonomous manner. Epifluorescence time-lapse experiments performed on the anterior endoderm of *Tg(sox17: EGFP)* host embryos transplanted with rhodamine-labeled donor cells (magenta). (A-C) *gpc4* mutant donor cells transplanted into wild-type *Tg(sox17: EGFP)* hosts. (D-F) Wild-type donor cells transplanted into *gpc4* mutant hosts (Movies 4 and 5). (A,A′,D,D′) Representative still images of anterior endoderm from movies. N, notochord; A, anterior; P, posterior; ML, medial-lateral. (B,C,E,F) Representative tracks delineate routes of migration of donor (B,E, magenta) and host (C,F, green) endodermal cells. (G,H) Total and net speeds of convergence and extension movements by donor (magenta) and host (green) endodermal cells. *n*=3 embryos per group. The number of endodermal cells tracked is indicated in the graph. #*P*>0.05; Student's *t*-test.

(mes/end boundary) (Fig. 5A,A′). These results are consistent with the previous finding that ECM fibrils are present at tissue boundaries (Latimer and Jessen, 2010). Notably, the assembly of Fn around the endoderm was fairly weak when compared with that at the ect/mes boundary (Fig. 5A,A′). By 4s, Fn assembly at both boundaries was much stronger than at TB (Fig. 5A,C). In *gpc4* mutants, the pattern of Fn assembly was similar to that in control

siblings (Fig. 5A-D). By assessing the relative intensity of Fn, we found that relative to control siblings, *gpc4* mutants had a significant increase in Fn fluorescence intensity, at both the ect/mes and mes/end boundaries (Fig. 5A-E). Additionally, the increase in Fn assembly in *gpc4* mutants resulted from an increase in expression of the Fn protein, as indicated by western blotting (Fig. 5F). Notably, overexpression of GFP-Gpc4 led to reduced Fn expression
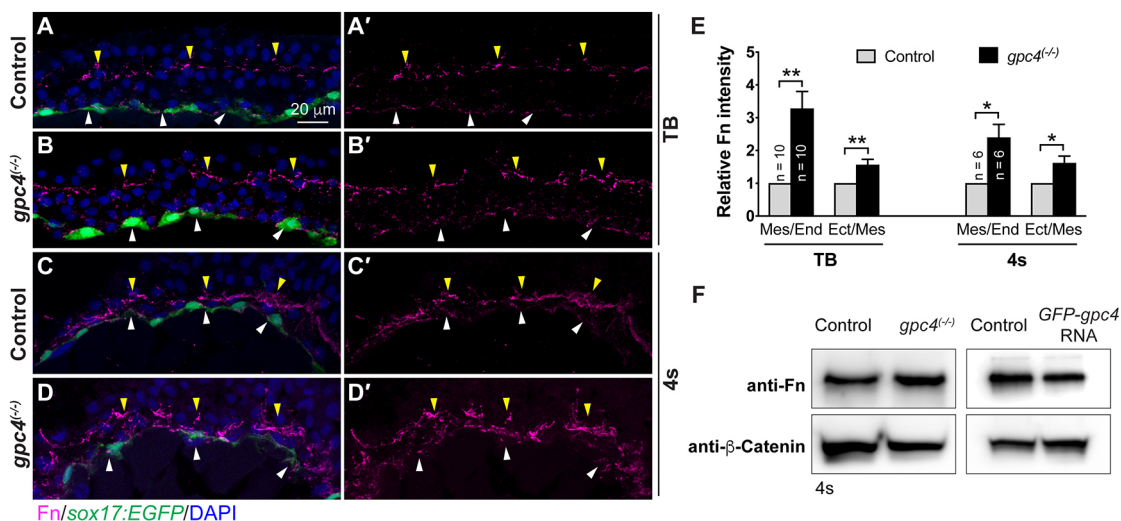
Fig. 5. Fibronectin (Fn) expression is increased in *gpc4* mutant embryos and reduced in GFP-Gpc4 expressing embryos. (A-E) Immunostaining of transverse cryosections for Fn deposition. (A-D′) Representative confocal *z*-stack images showing Fn (magenta) and nuclei (DAPI, blue) in embryos indicated. Fn assembly at mes/end (white arrowheads) and ect/mes (yellow arrowheads) boundaries. (E) Relative Fn intensity at mes/end and ect/mes boundaries in control and *gpc4* mutant embryos. The number of embryos analyzed is shown in the graph. (F) Western blot showing the expression of Fn and β-catenin (internal control) in embryos indicated. **P<0.01, *P<0.05; Student's *t*-test.

(Fig. 5F), which could be responsible for the rescue effect in *gpc4* mutants (Fig. S3). Analysis of Lam assembly in control embryos showed a much more diffuse expression pattern in all germ layers at the TB stage (Fig. S5A), but a concentration of signal at the mes/end boundary at the 4s stage (Fig. S5C). In *gpc4* mutants, Lam assembly was higher at both the mes/end boundary and the non-endoderm region (Fig. S5B,D,E). These results indicate that Gpc4 limits levels of both Fn and Lam to levels needed for efficient for migration of the anterior endodermal cells.

Next, we sought to determine whether increased ECM assembly is the cause of endoderm migration defects. First, qRT-PCR was performed on embryos at TB and 4s to assess expression of the *fn1a*, *fn11b*, *lama1*, *lamb1* and *lamc1* genes, which have been shown to be expressed in the zebrafish blastula and gastrula (Latimer and Jessen, 2010; Parsons et al., 2002; Zinkevich et al., 2006). We found that *lama1*, *lamb1a*, *lamc1* and *fn1a* are expressed at relatively high levels, whereas *lamb1b* and *fn1a* are expressed very low levels (Fig. S6A). Second, the effects of previously published MOs (Latimer and Jessen, 2010; Parsons et al., 2002; Zinkevich et al., 2006) were tested. Injection of one MO targeting *lama1*, *lamb1a* or *lamc1* significantly reduced Lam assembly at 4s (Fig. S6B,B′ and not shown), and injection of *fn1a* MO reduced Fn protein expression at this time (Fig. S6C). Notably, injection of these MOs individually at a high dose (10 ng) did not cause endodermal defects (Fig. S6D-F,J), whereas injection of a combination of MOs targeting both *fn1a* and *lama1* or *lamb1a* led to a widened endodermal sheet (Fig. S6G-I,K, not shown). Thus, not only an increase in ECM assembly, as observed in *gpc4* mutants, but also a decrease in the expression of both Fn and Lam, affects normal endoderm CE. Notably, injecting a subdose of *lamb1a* and *fn1a* MOs that cause mild endodermal defects partially rescued the endodermal defects in *gpc4* mutants (Fig. 6). Taken together, these data suggest that proper expression levels of ECM proteins are crucial for endoderm CE, and that the increased Fn and Lam expression in *gpc4* mutants at least partially contributes to defects in endodermal migration.

## Enhanced assembly of the ECM impairs the migration of endodermal cells

To directly test the impact of enhanced ECM assembly on endodermal migration, we manipulated the function of matrix metallopeptidase isoforms 14a and 14b (Mmp14a/b), which are expressed in the gastrula and have the ability to degrade Fn in the zebrafish gastrula (Coyle et al., 2008; Latimer and Jessen, 2010). We used previously validated MOs to suppress expression of the

mmp14a and *mmp14b* genes. In embryos injected with *mmp14a/ mmp14b* MOs targeting protein translation (ATG MOs), the assembly of both Fn and Lam was increased, including in the region surrounding the endoderm (Fig. S7A,B and data not shown), and the anterior endodermal sheet was significantly widened (Fig. S7C-E), as in *gpc4* mutants (Fig. 1A,B). We also injected embryos with a second set of MOs that disrupt *mmp14a/ mmp14b* splicing (SP MOs) (Coyle et al., 2008; Latimer and Jessen, 2010) and found that these morphants also produced a widened endodermal sheet, an effect that was partially suppressed by co-injecting *mmp14a/mmp14b* RNAs (Fig. S7F-H,L). Furthermore, these two sets of MOs have synergetic effects in endoderm CE (Fig. S7I-K,M). Collectively, these data indicate that enhanced ECM assembly due to the suppression of Mmp14a and Mmp14b impairs endoderm migration.

To further characterize the behaviors of endodermal cells in *mmp14a/mmp14b*-deficient embryos, we performed epifluorescence time-lapse experiments. Cell tracking showed that similar to *gpc4* mutant embryos, endodermal cells in *mmp14a/mmp14b* morphants migrated in a zig-zag pattern and had a significant reduction in net speed and the persistence index of CE (Fig. 7A-E). These data indicate that *mmp14a/mmp14b*-depleted endodermal cells migrate less efficiently than their wild-type counterparts. Furthermore, monitoring the actin dynamics of *Tg(sox17:GFP-UTRN)* showed that similar to *gpc4* mutant embryos, actin-rich protrusions in *mmp14a/mmp14b*-deficient endodermal cells were greater in number, smaller and shorter lived, and extended non-directionally (Fig. 7F-K). Taken together, these data suggest that suppression of *mmp14a/mmp14b* expression disrupts the migration of endodermal cells at early segmentation.

Gpc4 and Mmp14a/Mmp14b act synergistically to facilitate endodermal migration

The striking phenotypic similarities (increased ECM assembly and defective endodermal migration) between *gpc4* mutant and *mmp14a/mmp14b*-deficient embryos suggested that the encoded proteins can interact genetically to influence endodermal migration. Thus, we assessed the effects of loss of both *gpc4* and *mmp14a/ mmp14b* on endodermal migration. Embryos derived from crosses of *gpc4 Tg(sox17:EGFP)* heterozygous fish were injected with a sub-optimal dose of *mmp14a/mmp14b* ATG MOs (5 ng each). MO injection caused mild endodermal defects in wild-type and heterozygous *gpc4* embryos, and significantly stronger defects in *gpc4* mutant embryos (Fig. S8). The latter were stronger than
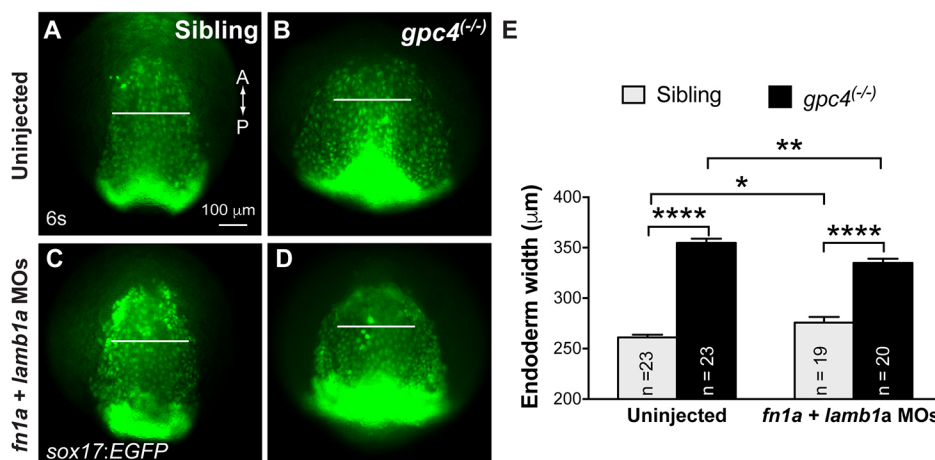
Fig. 6. Endodermal defects in *gpc4* mutants are suppressed by knocking down *fn1a* and *lamb1a*. (A-D) Epifluorescence still images of the anterior region of the endodermal sheet in 6s embryos derived from crossing of *gpc4*/ *Tg(sox17:EGFP)* heterozygous fish injected with or without MOs targeting *fn1a* and *lamb1a* (5 ng each). Anterior-dorsal view. White lines of equivalent length indicate width of the anterior endodermal sheets. A, anterior; P, posterior. (E) Average width of anterior endodermal sheet in embryos shown in A-D. Number of embryos analyzed in each group is indicated. *P<0.05, **P<0.01, ****P<0.0001; Student's *t*-test.
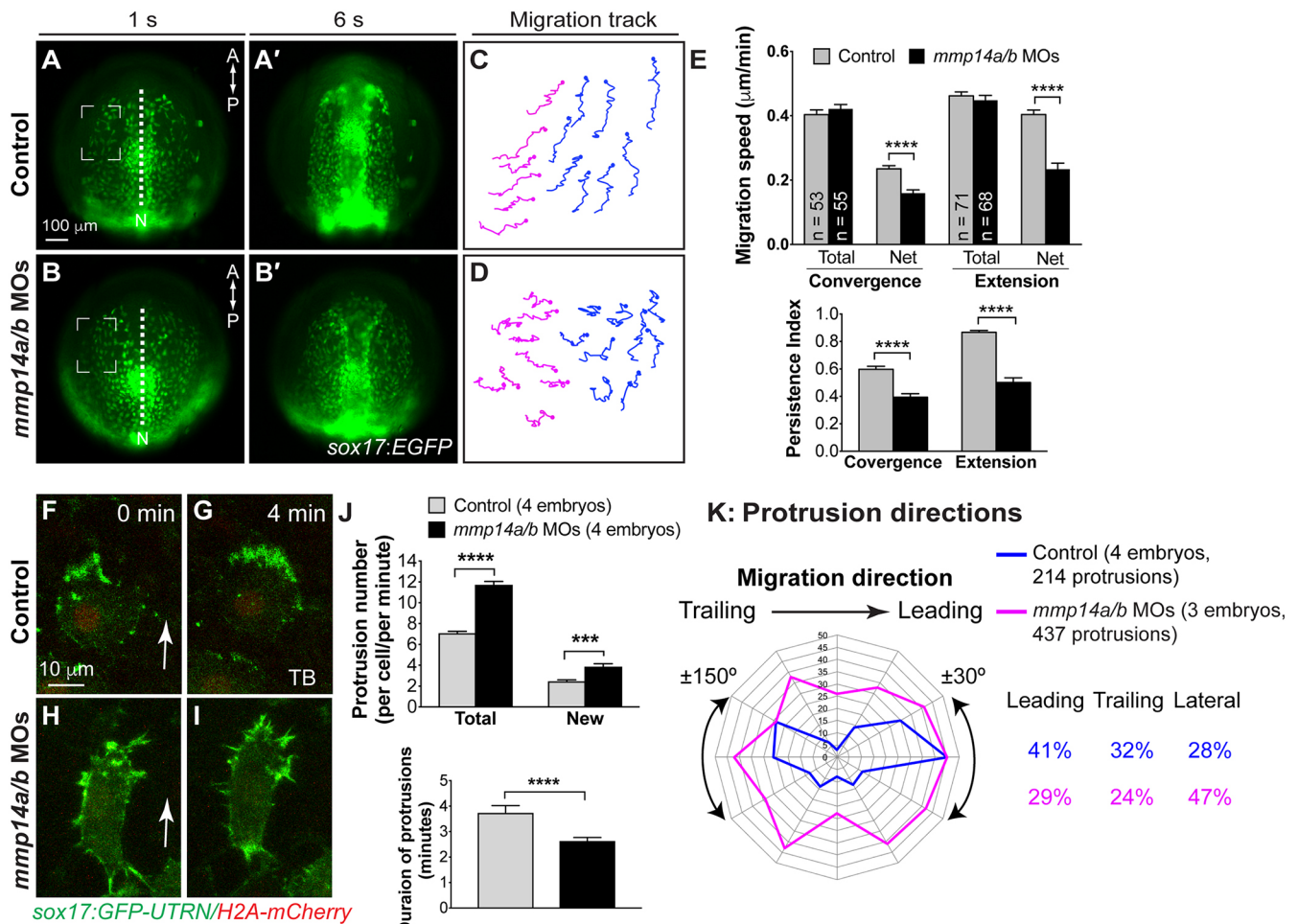
Fig. 7. Mmp14a and Mmp14b are required for convergence and extension movements of the anterior endodermal cells. (A-E) Epifluorescence time-lapse experiments for indicated embryos (Movie 6). (A-B′) Still images from movies at 1s and 6s. Dashed squares denote regions in which cells were analyzed. A, anterior; P, posterior. (C,D) Representative migration tracks of anterior endodermal cells in A and B. Blue and magenta tracks represent cells that migrated primarily in the anterior and medial directions, respectively. (E) Total and net speeds of convergence and extension movements, persistence index of cell migration, for the entire lengths of movies, in the embryos indicated (five embryos per group). The numbers of cells analyzed are indicated in the graph. ****P<0.0001; Student's t-test. (F-K) Actin dynamics as assessed by confocal time-lapse imaging of anterior endodermal cells expressing GFP-UTRN in the embryos indicated. (F-I) Representative confocal still images at 0 and 4 min (Movie 7). Arrows indicate direction of migration. (J) Total number (in each endodermal cell at 1 min intervals for the imaging period, 671 protrusions from six control cells, 926 protrusions from six morphant cells), newly formed protrusions (in each endodermal cell per minute, 198 protrusions in six control cells and 280 protrusions in six morphant cells) and duration of protrusions (35 protrusions from six control cells, 34 protrusions from six morphant cells). ***P<0.001; ****P<0.0001; Student's t-test. (K) Direction of protrusions relative to the direction of cell migration in sibling and mmp14a/b MOs-injected embryos (2 min intervals, grouped into 30° sectors). Percentage of protrusions in different directions (leading, ±30°; trailing, ±150°; lateral, ±30-150°) is shown.

expected for an additive effect, suggesting that the interaction between Gpc4 and Mmp14a/Mmp14b in regulating endoderm migration is synergistic.

To further investigate how Mmp14 and Gpc4 interact, we assessed the relative expression levels of *mmp14a* and *mmp14b* by qRT-PCR. We found that in wild-type embryos the expression level of *mmp14b* is much greater than that of *mmp14a* (25-fold at TB, 10-fold at 4s, data not shown). Notably, when compared with their control siblings, *gpc4* mutants expressed much less *mmp14b* at both TB and 4s; *mmp14a* expression was largely unchanged at TB but reduced at 4s (Fig. 8A). Thus, we postulated that overexpressing Mmp14 could rescue endoderm defects in *gpc4* mutants by reducing ECM expression. Indeed, injection of small doses of *mmp14a/b* RNAs (20+30 pg) reduced the expression of Fn (Fig. 8B). Notably, we found injecting *mmp14b* RNA alone (30 pg, did not cause endoderm phenotypes) partially rescued endodermal defects in *gpc4* mutants (Fig. 8C-G). This might be due

to the fact that *mmp14b* is the predominant isoform. However, we cannot inject a higher dose of *mmp14a* and *mmp14b* RNAs because they impair endoderm CE (not shown). Taken together, these data suggest that Gpc4 regulates the expression of Mmp14a/MMp14b, thereby maintaining levels of ECM assembly needed for endoderm CE (Fig. 8H).

DISCUSSION
Glypican 4 is required for efficient endodermal migration during segmentation
HSPGs have been implicated in many developmental processes, including cell movement during gastrulation as well as development of the heart and nervous system (Poulain and Yost, 2015). Gpc4 is an HSPG that regulates CE movements (Ohkawara et al., 2003; Topczewski et al., 2001) and migration of the lateral line primordium (LLP) (Venero Galanternik et al., 2016). In this study, we show that Gpc4 is required for the migration of anterior
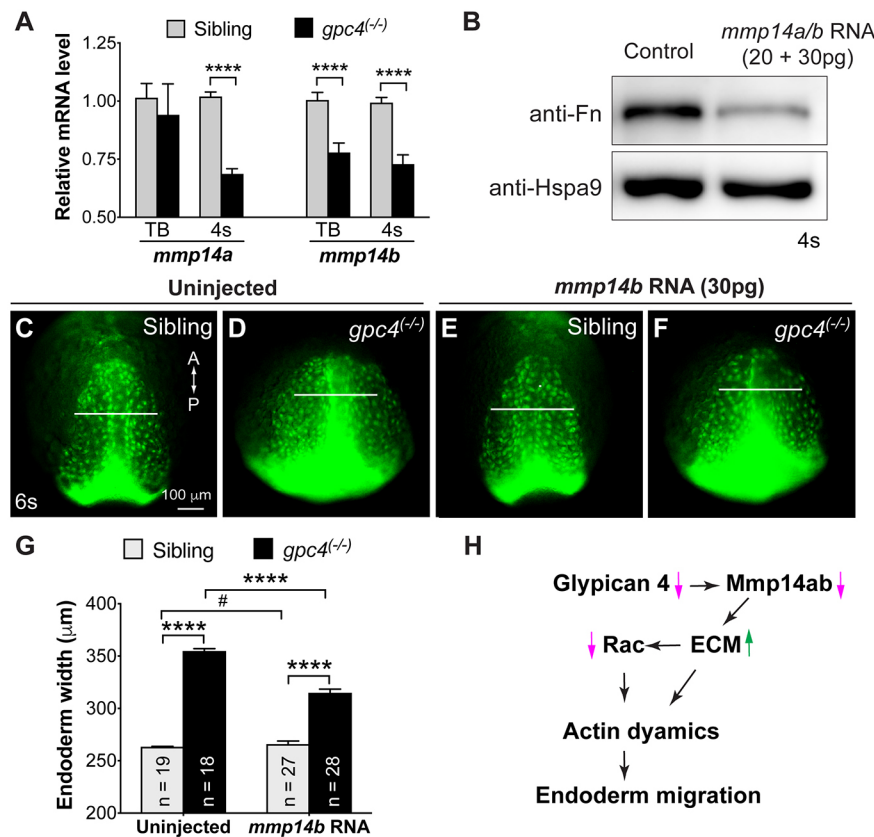
Fig. 8. Gpc4, Mmp14a and Mmp14b interact to regulate endodermal migration. (A) Relative mRNA levels of *mmp14a* and *mmp14b* when compared with *eef1a* in embryos indicated, as determined by qRT-PCR. ****$P<0.0001$, Student's *t*-test. (B) Western blot showing the expression levels of Fn and heat-shock protein 9 (Hspa9, internal control) in control and *mmp14a/b* RNA-injected embryos. (C-F) Epifluorescence still images of the anterior region of the endodermal sheet in 6s embryos derived from crossing *gpc4/Tg(sox17:EGFP)* heterozygous fish injected with or without *mmp14b* RNA. White lines of equivalent length indicate the width of the anterior endodermal sheet. A, anterior; P, posterior. (G) Average width of anterior endoderm. The numbers of embryos analyzed is indicated. ****$P<0.0001$, #$P>0.05$; Student's *t*-test. (H) Proposed model for how Gpc4 regulates the migration of endodermal cells at early segmentation. Magenta arrows indicate decreases in expression; green arrow indicates increase in expression.

endodermal cells during segmentation, revealing a new role for this protein. Our live imaging revealed that during early segmentation, endodermal cells migrate individually, with endodermal cell populations in separate regions migrating in the medial and anterior directions, respectively, narrowing the sheet along its mediolateral axis and extending it along the anteroposterior axis. In *gpc4* mutants, the overall motility of endodermal cells is largely unaffected but the efficiency of their migration is significantly impaired, as is evident from their non-directional pattern and reduced persistence of migration in these embryos (Fig. 1). Furthermore, the migration defects of endodermal cells in *gpc4*-deficient embryos are due to an inability to maintain actin-rich protrusions in the leading edge of the cell, likely as a result of reduced Rac1 activity and a loss of polarized Rac1 activation (Figs 2 and 3). These results indicate that Gpc4 is required to promote the spatial activation of Rac1 in endodermal cells, to enable directed cell migration. Notably, Gpc4 has been shown to control the planar polarity of mesodermal cells to enable gastrulation movements (Topczewski et al., 2001). However, how it impacts the migratory behaviors of mesoderm cells remains unknown. Additionally, in embryos with reduced levels of HSPGs, cells of the posterior LLP (pLLP) also extend ectopic cell protrusions in multiple directions (Venero Galanternik et al., 2016), potentially contributing to their migratory defects. Given this common phenotype, it would be interesting to determine whether Gpc4 modulates the migration of other cell types and, if so, whether it uses similar mechanisms.

The role of Wnt/PCP signaling in endoderm migration
Like other HSPGs, Gpc4 is a cell-surface-bound protein that interacts extracellularly with various secreted molecules, including Wnts, Bmps and FGFs, by regulating the availability of these signaling factors or by acting as a co-receptor for these molecules. In the gastrulating mesoderm, Gpc4 interacts with Wnt11 to promote Wnt/PCP signaling for CE (Ohkawara et al., 2003; Topczewski et al., 2001). A study using a dominant-negative Dishevelled protein (DvlΔDEP) and MOs to knock down multiple Wnt ligands implicated Wnt/PCP signaling in endoderm convergence at late segmentation (Matsui et al., 2005). Thus, it is possible that Wnt/PCP signaling is involved in endoderm CE during segmentation and that Gpc4 acts through Wnt/PCP signaling to regulate endoderm migration. However, endoderm migration is not affected in the absence of *vangl2*, a core Wnt/PCP gene, mutations in which cause CE defects similar to those observed in *gpc4* mutants during gastrulation (Fig. S2). Furthermore, analysis of cell shape in the anterior endoderm at 4s revealed that wild-type cells do not have uniform patterns of cell polarity (Fig. S4), a hallmark of gastrulating mesoderm cells (Gray et al., 2011). Instead, endodermal cells in different locations exhibited distinct shapes, and these were not affected by *gpc4* deficiency (Fig. S4). These data suggest that *vangl2* and *gpc4* have distinct roles in endoderm migration, and that Wnt/PCP signaling is not involved in the migration of anterior endodermal cells at this stage.

Notably, Gpc4 and Vangl2 also have separate roles in other processes. For example, Vangl2 but not Gpc4 is required for the migration of branchial motor neurons (Jessen et al., 2002). In contrast, Gpc4, but not Vangl2, is required for palate morphogenesis (Sisson et al., 2015) and pLLP migration (Venero Galanternik et al., 2016). Vangl2 and Gpc4 also play distinct roles in ECM assembly and cell-cell adhesion (Dohn et al., 2013), in MTOC polarization in gastrulating lateral mesodermal cells (Sepich et al., 2011), in membrane recruitment by Gpr125 (Li et al., 2013), and in recruitment of mutated in colorectal cancer (MCC) as a downstream effector (Young et al., 2014). Thus, Gpc4 and Vangl2 have distinct functions in a variety of processes during embryogenesis.

Glypican 4 modulates endodermal migration in a non-cell-autonomous manner by limiting assembly of the extracellular matrix

Gpc4 can function in non-cell-autonomous fashion. Recently, it was shown that, in the pLLP, Gpc4 affects the expression of sonic hedgehog (Shh) during the development of muscle cells, which express the chemokine that directs LLP migration (Venero Galanternik et al., 2016). Similarly, Gpc4 regulates the specification and differentiation of cardiac mesoderm by attenuating Wnt and Bmp signaling in the anterior lateral plate mesoderm where cardiac cells are located (Strate et al., 2015). In the zebrafish gastrula, *gpc4* is expressed ubiquitously (Topczewski et al., 2001). However, the autonomous role of Gpc4 in regulating the polarity and migration of mesoderm cells has not yet been tested. In this study, we found that *gpc4* is also expressed in the endoderm (Fig. S1). Furthermore, our studies show that *gpc4* mutant endodermal cells migrated normally in a wild-type environment, whereas wild-type endodermal cells failed to migrate in a *gpc4*-mutant environment (Fig. 4). This indicates that Gpc4 exerts effects on the environment to promote endodermal migration rather than affecting the endoderm directly. However, it does not exclude the possibility that Gpc4 has additional roles in the endoderm.

Proper endoderm migration during gastrulation requires interactions between the ECM and integrins, which are regulated by chemokine signaling (Nair and Schilling, 2008). Notably, increased assembly of the ECM component Fn is observed in *gpc4* mutants during gastrulation (Dohn et al., 2013). We reasoned that such changes in ECM assembly could affect integrin signaling, which would in turn affect endoderm migration. Indeed, we found that both Fn and Lam fibers assemble at the ectoderm/mesoderm boundary, between the endoderm/mesoderm and in the area surrounding the endoderm at the TB and 4s stages. However, in the absence of Gpc4, the assembly of Fn and Lam was significantly increased, particularly in the region surrounding the endoderm, and expression of Fn was increased (Fig. 5, Fig. S5). Furthermore, suppressing expression of *fn1a* and *lamb1a*, major isoforms that are expressed at early segmentation, can partially rescue endodermal defects in *gpc4* mutants (Fig. 6). Considering that overexpressing GFP-Gpc4 reduced Fn expression (Fig. 5F), it appears that Gpc4 can modulate ECM expression. Collectively, our data indicate that Gpc4 is required to create an environment conducive to endodermal migration by limiting the assembly of ECM components. In the future, determining which signaling molecules directly promote proper migration of endodermal cells during segmentation will help to establish the network that governs morphogenesis of the anterior endoderm.

ECM assembly may play a role in endoderm migration

The ECM is crucial for many cellular processes during development (Bonnans et al., 2014; Rozario and DeSimone, 2010). Increasing evidence is showing that the ECM serves not only as a physical barrier and supportive structure, but also as an environment in which cell signals can regulate cell specification, differentiation, growth and survival. In addition, the ECM constitutes a crucial component of the cell migratory machinery, influencing cell motility and cell-ECM adhesion through interactions with integrin receptors. For example, the ECM component Fn is required for the migration of gastrulating mesodermal cells in *Xenopus* and zebrafish (Latimer and Jessen, 2010; Marsden and DeSimone, 2001, 2003). Although reducing the expression of either Fn or Lam did not affect endoderm migration, removing both proteins impaired endoderm migration (Fig. S6), consistent with the finding that interfering with integrin signaling disrupts endoderm migration (Nair and Schilling, 2008).

In this study, we show that endoderm migration is impaired in both *gpc4* mutants and *mmp14a/b* MOs-injected embryos, likely due to increased ECM assembly in areas surrounding the endoderm. Thus, endoderm migration relies on optimal assembly and localization of the ECM. Consistent with the findings on endoderm migration, the migration of cardiac precursors during heart-tube formation depends on proper levels of Fn expression in the cardiac mesoderm, with both reduced and elevated Fn expression impairing myocardial migration (Garavito-Aguilar et al., 2010; Trinh and Stainier, 2004). Thus, precise regulation of the expression and assembly of ECM components is required for several developmental processes during organ formation.

Gpc4 and Mmp14 interact to facilitate endoderm migration

Increased ECM assembly and similarities in endodermal defects in *gpc4* mutant *mmp14a/mmp14b* morphants suggest that these genes may interact. Indeed, our genetic synergy experiments, in which *mmp14a/mmp14b* expression was suppressed in *gpc4* mutant embryos, revealed that Gpc4 and Mmp14 interact to regulate endoderm migration during segmentation (Fig. S8). Furthermore, we found that in *gpc4* mutants, the levels of *mmp14a/mmp14b* transcription are reduced (Fig. 8), an effect that could potentially be responsible for the observed increased ECM expression and endodermal defects. Thus, we reduced the expression of ECM proteins by injecting embryos with *mmp14a/mmp14b* RNAs (Fig. 8B). We found that injection with high doses of RNAs impaired endodermal CE (not shown), producing a phenotype similar to that observed in embryos injected with both *fn1a* and *lamb1a* MOs (Fig. S6). Thus, eliminating expression of ECM also impairs endoderm migration. These data suggest that endoderm formation relies on proper expression and assembly of ECM components. However, injection of a low dose of the *mmp14b* RNA, which produces minimal development defects, can partially rescued endodermal defects in *gpc4* mutant embryos, suggesting that Gpc4 acts through Mmp14a/Mmp14b to produce ECM levels appropriate for endodermal migration (Fig. 8). The interaction of these two proteins in promoting endoderm migration are consistent with a previously reported genetic interaction between Gpc4 and Mmp14 in mesoderm migration during gastrulation (Coyle et al., 2008). Thus, future studies will investigate how Gpc4 influences Mmp14 expression.

Proteoglycans have been implicated in tumorigenesis (Theocharis and Karamanos, 2017). In particular, mutant forms of glypican 3, an isoform of Gpcs, plays a crucial role in hepatocellular carcinoma (Montalbano et al., 2017). Moreover, MMP14 is a major metalloproteinase that regulates the invasiveness of cancer cells (Turunen et al., 2017). Thus, our current study investigating the interaction of Gpc4 with Mmp14 in zebrafish could provide insight into mechanisms underlying the role of glypicans in cancer progression.

In summary, our work shows that during early segmentation, endodermal cells migrate individually toward the anterior and dorsal regions of the embryo, contributing to CE. Such endoderm migration requires Gpc4, which regulates Rac1 activation to provide directionality to migrating endodermal cells. Gpc4 regulates endoderm migration in a non-cell-autonomous manner, by interacting with Mmp14 to limit deposition of ECM components (Fig. 8H). Thus, in addition to providing insight into the role of Gpc4 during endoderm morphogenesis in embryonic development, our results have significant implications for our understanding of other developmental processes that depend on Gpc4.

DEVELOPMENT

MATERIALS AND METHODS

Zebrafish strains and maintenance

Zebrafish were maintained as described previously (Xu et al., 2011). Animal protocols were approved by the University of Iowa Animal Care and Use Committee. Unless otherwise specified, embryos were obtained by natural spawning and staged according to morphological criteria or hours post fertilization (hpf) at 28 or 32°C, as described previously (Kimmel et al., 1995). The following zebrafish lines were used: AB*/Tuebingen, NHGRI-1 (LaFave et al., 2014), *Tg(sox17:GFP-UTRN)* (Woo et al., 2012), *Tg(sox17: EGFP)* (Mizoguchi et al., 2008), *knypek^{fr6}* (*gpc4* mutant) (Topczewski et al., 2001) and *trilobite^{uv67}* (*vangl2* mutant) (Li et al., 2013). We also generated *Tg(sox17:H₂AmCherry)* and *Tg(sox17:memGFP)* using a Tol2-based Multi-Site Gateway system (Invitrogen) (Kwan et al., 2007; Villefranc et al., 2007) as described previously (Ye et al., 2015). To genotype *gpc4* mutant embryos, genomic DNAs were amplified using the following primers: forward, 5′-GACCAATCAAGGCTTATCTTC; reverse, 5′-AACTAACAATTAAGGAGGGCTA. PCR amplicons were distinguished by enzymatic digestion with *Cla*I: wild-type DNAs produced two bands at 323 bp and 206 bp; mutant DNAs produced a single band at 529 bp. To genotype *vangl2* mutant embryos, genomic DNAs were amplified with the following primers: forward, 5′-ATTCCCTGGAGCCC-TGCGGGAC; reverse, 5′-AGCGCGTCCACCAGCGACACAGC. PCR amplicons were digested with *Alu*I: wild-type DNAs produced bands at 59 bp and 212 bp; mutant DNAs produced bands at 17 bp, 59 bp and 195 bp.

Generation of a GFP-Gpc4 construct, cloning of Mmp14b, and injection of RNAs and morpholinos (MOs)

GFP-Gpc4 was generated by inserting the open reading frame sequence of EGFP after the predicted cleavage site of the N-terminal signal peptide (MKMIVVFTVCMSVVVLASAQADQ) of Gpc4, which was sub-cloned into a gateway pCS2dest vector (Kwan et al., 2007). Full-length *mmp14b* (NM194414.1) was amplified from a cDNA library generated from 18 hpf embryos using the following primers: forward, 5′-TTATGAATTCAATG-ATCTGGAGCGGGTTTACGAGGC; reverse, 5′-GCCTCTCGAGTTAA-ACCTTGTCCAGTAGGGAGCGTT. The amplicon was cloned into a the *Eco*RI and *Xho*I sites of the pCS2-Myc vector. Capped mRNAs were synthesized using the mMessage mMachine kit (Ambion). The RNAs encoding the following genes were used: *sox32* (Stafford et al., 2006), *GFP-gpc4*, *Myc-mmp14b*, *mmp14a* (Coyle et al., 2008) and *GFP-PDB* (the Rac1-binding domain of p21-activated kinase) (Miller and Bement, 2009; Woo et al., 2012). Previously validated MOs targeting the following genes were used: *mmp14a* ATG, 5′-GACGGTACTCAAGTCGGGACACAAA; *mmp14b* ATG, 5′-GAACCCGCTCCAGATCATTTTTCGC; *mmp14a* splice, 5′-TAAGACTGGGCGAGACTTACGAGAG; *mmp14b* splice, 5′-ATGTTGGAAAACTGGCTTACTCTAG (Coyle et al., 2008); *lamb1a*, 5′-TATTTCCAGTTTCTTTCTTCAGCGG; *lamc1*, 5′-TGTGCCTTTTG-CTATTGCGACCTC (Parsons et al., 2002); *lama1*, 5′-ATAAAGCTAA-AGCTGTGCTGAAATC (Zinkevich et al., 2006); *fn1a*, 5′-TTTTTTCACAGGTGCGATTGAACAC (Trinh and Stainier, 2004); and *p53*, 5′-GCGCCATTGCTTTGCAAGAATTG (Robu et al., 2007). mRNA and MOs were injected at the one-cell stage, at the doses indicated in the figure legends. All the MOs were co-injected with 1.5 ng *p53* MO.

Whole-mount *in situ* hybridization, immunofluorescence assay and western blotting

Digoxigenin-labeled antisense RNA probes targeting *sox17* (Alexander et al., 1999), *foxa2* (Odenthal and Nüsslein-Volhard, 1998), *gpc4* (Topczewski et al., 2001) and *vangl2* (Jessen and Solnica-Krezel, 2004) were synthesized by *in vitro* transcription. *In situ* hybridization was performed as previously described (Lin et al., 2005; Thisse and Thisse, 2008). After *in situ* hybridization, embryos were re-fixed in 4% paraformaldehyde (PFA) and sectioned at 10 μm, as described previously (Barthel and Raymond, 1990). Immunofluorescence staining for GFP was performed as described previously (Trinh and Stainier, 2004) using an anti-GFP antibody (1:300, sc-8334, Santa Cruz Biotechnology). For detecting fibronectin (Fn) and laminin (Lam) expression in *gpc4* mutants, embryos derived from *kny^{fr6}/Tg(sox17:EGFP)* heterozygous crosses were collected and fixed overnight in 4% PFA at 4°C. Mutant embryos were identified based on morphological phenotypes, and

pairs of mutant and control sibling embryos were mounted in the same block. Blocks were sectioned at 14 μm, as described above. Immunofluorescence staining was carried out in a serum-free solution (1% BSA, 2% DMSO, 0.1% Triton X-100 in PBS) using anti-fibronectin (1:300, F3648, Sigma-Aldrich), anti-laminin (1:300, RB-082-A, ThermoFisher Scientific) and an Alexa Fluor A568-conjugated goat anti-rabbit secondary antibody (1:400, A-11036, Invitrogen). Sections were counterstained with 4′,6-diamidino-2-phenylindole (DAPI, 0.2 μg/ml, ThermoFisher Scientific) for 10 min and mounted in 90% glycerol/PBS medium containing 0.2% propyl gallate. For western blotting, embryos were de-yolked as previously described (Link et al., 2006) and lysed in 2× SDS loading buffer (2 μl per embryo). Volumes of lysate equivalent to 10-15 embryos were loaded. The following antibodies were used for immunoblotting: anti-fibronectin (1:800, F3648, Sigma-Aldrich), anti-β-catenin (1:1000, C7207, Sigma-Aldrich) and anti-Hspa9/mortalin (1:1000, P38647, NeuroMab).

Fluorescence-activated cell sorting (FACS), RNA isolation and quantitative real-time PCR

18s *Tg(sox17:GFP)* embryos were de-yolked by pipetting through 200 μl pipette tips in Ca²⁺-free Ringer's solution, and cells were freed from the ECM by incubation with Liberase Blendzyme (0.26 UI/ml, Roche) in PBS at 32°C for 60 min. The cells were next washed and sorted for GFP signal using a FACS Aria II instrument (Becton Dickinson). RNA was then generated from the GFP⁺ cells and GFP⁻ cells, and cDNAs were synthesized using the iScript Reverse Transcription kit (Bio-Rad Laboratories). These cDNAs were then quantitated using real-time PCR and the iQ SYBR Green Supermix (Bio-Rad Laboratories). Primers used to amplify *gpc4*, *vangl2*, *vangl1*, *foxa2*, *fn1a*, *fn1b*, *lama1*, *lamb1a*, *lamb1b*, *lamc1*, *mmp14a*, *mmp14b* and *eef1a1a* are listed in Table S1.

Endoderm transplantation

Endoderm transplantation was carried out as described previously (Chung and Stainier, 2008; Stafford et al., 2006; Ye and Lin, 2013). Donor embryos at the one-cell stage were injected with 250 pg of *sox32* RNA to confer an endodermal identity to all cells, and with 0.2% rhodamine-dextran (70,000 MW, lysine-fixable, Invitrogen) as a lineage tracer. At 1 k-high stage, 30-50 donor cells were transplanted into the host embryos, along the blastoderm margin. Host embryos were screened for rhodamine-labeled donor cells in the anterior endoderm before time-lapse imaging was initiated. When *gpc4 mutant* embryos were used as either donors or hosts, all embryos were genotyped for the *knypek^{fr6}* allele.

Rac activity assay

GFP-PDB, a probe of Rac1 activity, was expressed in a mosaic fashion by endoderm transplantation as described above. Embryos derived from crossing heterozygous *gpc4* mutant zebrafish served as both donors and hosts, and their genotypes were determined. Donor embryos were injected with RNAs encoding *sox32* (250 pg) and *GPP-PDB* (200 pg), as well as 0.2% rhodamine-dextran. Transplantation was performed as described above. Following transplantation, at TB, host embryos in which transplanted cells were detected were embedded in 0.7% low-melting agarose and confocal time-lapse imaging was performed on the anterior endoderm using an inverted laser-scanning confocal microscope (LSM700, Carl Zeiss) with a LD C-Apo 40×/NA 1.1 water objective. Approximately 16 μm z-stacks were acquired at 2 μm intervals every 10 s using the following settings: 512×512 pixels, speed 7, 2 averaging. Images were processed and analyzed using Fiji software as described previously (Woo et al., 2012). Briefly, maximum projections were obtained from a single time frame and converted to 32-bit format. GFP-PDB and rhodamine-dextran images were separated and the background was set to NaN. Images were normalized to their respective 'median' value using the 'divide' tool. Ratiometric images were generated by dividing the PDB image by the dextran image using the 'image calculator' tool. The ratio of PDB:dextran was obtained by measuring 'the mean gray' value of the cell region outlined using the polygon selection tool.

Microscopy, time-lapse imaging and image processing

For still epifluorescence images, live or fixed embryos were mounted in 2.5% methylcellulose and photographed using a Leica DMI 6000

microscope with a 5×/NA 0.15 or 10×/NA 0.3 objective. Whole-mount *in situ* hybridization and bright-field images were taken on a Leica M165FC stereomicroscope with a Leica DFC290 Color Digital Camera. *In situ* hybridization sections were mounted in 90% glycerol/PBS medium containing 0.2% propyl gallate and photographed using a Nikon Microphot-FX microscope. Confocal images were taken on a Zeiss inverted LSM700 laser-scanning confocal microscope with an EC Plan-Neo 40×/NA 1.3 oil or LD C-Apo 40×/NA 1.1 water objective. Z-stacks were acquired at 0.5 μm intervals using the following settings: 1024×1024 pixels, 8 speed, 4 averaging. For time-lapse imaging, embryos were embedded in 0.7% (for embryos aged before 10 hpf) or 1% (for embryos aged beyond 10 hpf) low melting-point agarose using glass-bottom dishes and images were captured in the anterior region of the endoderm at 25°C as described previously (Ye et al., 2015). Epifluorescence time-lapse imaging was performed on *Tg(sox17:EGFP)* embryos embedded in a dorsal-mount imaging mold, as previously described (Megason, 2009; Ye and Lin, 2013), at 5 min intervals with a 5×/NA 0.15 objective on a Leica DMI 6000 microscope. Confocal time-lapse imaging was performed on *Tg(sox17: GFP-UTRN)* embryos using a laser-scanning confocal inverted microscope (LSM700, Carl Zeiss) with a LD C-Apo 40×/NA 1.1 water objective. One or two endodermal cells were selected for imaging using regions of interest (ROI) for average 15 min. Approximately 15 μm z-stacks at 1.5 μm intervals (covering all endodermal cells) were captured every 10 s using the following settings: 512×512 pixels, 7 speed, 2 averaging.

Image analysis
All images of the same type were acquired using the same settings, processed using the MetaMorph or Fiji software, and edited and compiled using Adobe Photoshop and Adobe Illustrator software. Cell tracking was analyzed using the manual tracking plug-in of the Fiji software. Data were exported to Microsoft Excel and the speed, path and direction of cell migration were determined as previously reported (Lin et al., 2005; Ye and Lin, 2013). For protrusion analysis, maximum projections were generated using the Fiji software. The number of cellular protrusions that formed throughout each movie was counted manually. For each cell, the average value of three independent analyses was used for further statistical analysis. The duration (lifetime) of each protrusion was measured from the time at which a new protrusion was observed to the time at which it was retracted. To measure the direction of cell protrusions, z-stack images were rotated the direction of cell movement horizontally (0°C) and the angle of each protrusion relative to migration direction was assessed using by Fiji software. To assess changes in cell morphology, endodermal cells of interest were outlined, and the length (L) and width (W) were determined using Fiji software. To quantify the intensity of the Fn and Lam signals, maximum projection images were obtained from ∼10 μm z planes and converted into 32-bit images using Fiji software. 'Lower threshold' and 'upper threshold' were set to 50 and 255, respectively, and the background was set to NaN. The rectangular tool was used to define the region of interest (ROI) in *sox17:EGFP*-expressing endodermal and non-endodermal areas. The mean of the gray value and the area value (μm^2) where intensity was within the setting threshold range (50-255) were measured. These two values were then multiplied and the product was divided by the area (μm^2) of the ROI to obtain the average intensity. The intensity of at least two sections from similar regions of mutant and sibling embryos was calculated and averaged, with fold change in intensity calculated as relative intensity of mutant versus sibling embryos.

Statistical analysis
Data were compiled from two or three independent experiments and are presented as the mean±s.e.m. Statistical analyses were performed using the unpaired two-tailed Student's *t*-test with unequal variance. $P<0.05$ was considered significant. The numbers of cells and embryos analyzed in each experiment are indicated in the figure legends.

Competing interests
The authors declare no competing or financial interests.

Author contributions
Conceptualization: B.H., F.L.; Methodology: B.H., Y.G., L.D., S.W., J.T., J.R.J., F.L.; Software: B.H., Y.G., S.W., F.L.; Validation: B.H., F.L.; Formal analysis: B.H., Y.G., F.L.; Investigation: B.H., Y.G., L.D., J.T., F.L.; Resources: S.W., J.T., J.R.J., F.L.; Data curation: B.H., Y.G., L.D., F.L.; Writing - original draft: B.H., F.L.; Writing - review & editing: B.H., F.L.; Visualization: B.H., F.L.; Supervision: F.L.; Project administration: F.L.; Funding acquisition: F.L.

Supplementary information
Supplementary information available online at
http://dev.biologists.org/lookup/doi/10.1242/dev.163303.supplemental

References

Alexander, J., Rothenberg, M., Henry, G. L. and Stainier, D. Y. R. (1999). casanova plays an early and essential role in endoderm formation in zebrafish. *Dev. Biol.* **215**, 343-357.

Barthel, L. K. and Raymond, P. A. (1990). Improved method for obtaining 3-microns cryosections for immunocytochemistry. *J. Histochem. Cytochem.* **38**, 1383-1388.

Bonnans, C., Chou, J. and Werb, Z. (2014). Remodelling the extracellular matrix in development and disease. *Nat. Rev. Mol. Cell Biol.* **15**, 786-801.

Burkel, B. M., von Dassow, G. and Bement, W. M. (2007). Versatile fluorescent probes for actin filaments based on the actin-binding domain of utrophin. *Cell Motil. Cytoskelet.* **64**, 822-832.

Butler, M. T. and Wallingford, J. B. (2017). Planar cell polarity in development and disease. *Nat. Rev. Mol. Cell Biol.* **18**, 375-388.

Choe, C. P. and Crump, J. G. (2015). Dynamic epithelia of the developing vertebrate face. *Curr. Opin. Genet. Dev.* **32**, 66-72.

Chung, W.-S. and Stainier, D. Y. R. (2008). Intra-endodermal interactions are required for pancreatic beta cell induction. *Dev. Cell* **14**, 582-593.

Coyle, R. C., Latimer, A. and Jessen, J. R. (2008). Membrane-type 1 matrix metalloproteinase regulates cell migration during zebrafish gastrulation: evidence for an interaction with non-canonical Wnt signaling. *Exp. Cell Res.* **314**, 2150-2162.

Dohn, M. R., Mundell, N. A., Sawyer, L. M., Dunlap, J. A. and Jessen, J. R. (2013). Planar cell polarity proteins differentially regulate extracellular matrix organization and assembly during zebrafish gastrulation. *Dev. Biol.* **383**, 39-51.

Fico, A., Maina, F. and Dono, R. (2011). Fine-tuning of cell signaling by glypicans. *Cell. Mol. Life Sci.* **68**, 923-929.

Filmus, J., Capurro, M. and Rast, J. (2008). Glypicans. *Genome Biol.* **9**, 224.

Garavito-Aguilar, Z. V., Riley, H. E. and Yelon, D. (2010). Hand2 ensures an appropriate environment for cardiac fusion by limiting Fibronectin function. *Development* **137**, 3215-3220.

Gray, R. S., Roszko, I. and Solnica-Krezel, L. (2011). Planar cell polarity: coordinating morphogenetic cell behaviors with embryonic polarity. *Dev. Cell* **21**, 120-133.

Jessen, J. R. and Solnica-Krezel, L. (2004). Identification and developmental expression pattern of van gogh-like 1, a second zebrafish strabismus homologue. *Gene Expr. Patterns* **4**, 339-344.

Jessen, J. R., Topczewski, J., Bingham, S., Sepich, D. S., Marlow, F., Chandrasekhar, A. and Solnica-Krezel, L. (2002). Zebrafish trilobite identifies new roles for Strabismus in gastrulation and neuronal movements. *Nat. Cell Biol.* **4**, 610-615.

Kardash, E., Bandemer, J. and Raz, E. (2011). Imaging protein activity in live embryos using fluorescence resonance energy transfer biosensors. *Nat. Protoc.* **6**, 1835-1846.

Keller, R. (2002). Shaping the vertebrate body plan by polarized embryonic cell movements. *Science* **298**, 1950-1954.

Kimmel, C. B., Ballard, W. W., Kimmel, S. R., Ullmann, B. and Schilling, T. F. (1995). Stages of embryonic development of the zebrafish. *Dev. Dyn.* **203**, 253-310.

Kwan, K. M., Fujimoto, E., Grabher, C., Mangum, B. D., Hardy, M. E., Campbell, D. S., Parant, J. M., Yost, H. J., Kanki, J. P. and Chien, C.-B. (2007). The Tol2kit:

DEVELOPMENT

a multisite gateway-based construction kit for Tol2 transposon transgenesis constructs. *Dev. Dyn.* **236**, 3088-3099.

LaFave, M. C., Varshney, G. K., Vemulapalli, M., Mullikin, J. C. and Burgess, S. M. (2014). A defined zebrafish line for high-throughput genetics and genomics: NHGRI-1. *Genetics* **198**, 167-170.

Latimer, A. and Jessen, J. R. (2010). Extracellular matrix assembly and organization during zebrafish gastrulation. *Matrix Biol.* **29**, 89-96.

Li, X., Roszko, I., Sepich, D. S., Ni, M., Hamm, H. E., Marlow, F. L. and Solnica-Krezel, L. (2013). Gpr125 modulates Dishevelled distribution and planar cell polarity signaling. *Development* **140**, 3028-3039.

Lin, F., Sepich, D. S., Chen, S., Topczewski, J., Yin, C., Solnica-Krezel, L. and Hamm, H. (2005). Essential roles of G{alpha}12/13 signaling in distinct cell behaviors driving zebrafish convergence and extension gastrulation movements. *J. Cell Biol.* **169**, 777-787.

Link, V., Shevchenko, A. and Heisenberg, C.-P. (2006). Proteomics of early zebrafish embryos. *BMC Dev. Biol.* **6**, 1.

Marsden, M. and DeSimone, D. W. (2001). Regulation of cell polarity, radial intercalation and epiboly in Xenopus: novel roles for integrin and fibronectin. *Development* **128**, 3635-3647.

Marsden, M. and DeSimone, D. W. (2003). Integrin-ECM interactions regulate cadherin-dependent cell adhesion and are required for convergent extension in Xenopus. *Curr. Biol.* **13**, 1182-1191.

Matsui, T., Raya, A., Kawakami, Y., Callol-Massot, C., Capdevila, J., Rodriguez-Esteban, C. and Izpisua Belmonte, J. C. (2005). Noncanonical Wnt signaling regulates midline convergence of organ primordia during zebrafish development. *Genes Dev.* **19**, 164-175.

Megason, S. G. (2009). In toto imaging of embryogenesis with confocal time-lapse microscopy. *Methods Mol. Biol.* **546**, 317-332.

Miles, L. B., Mizoguchi, T., Kikuchi, Y. and Verkade, H. (2017). A role for planar cell polarity during early endoderm morphogenesis. *Biol. Open* **6**, 531-539.

Miller, A. L. and Bement, W. M. (2009). Regulation of cytokinesis by Rho GTPase flux. *Nat. Cell Biol.* **11**, 71-77.

Mizoguchi, T., Verkade, H., Heath, J. K., Kuroiwa, A. and Kikuchi, Y. (2008). Sdf1/Cxcr4 signaling controls the dorsal migration of endodermal cells during zebrafish gastrulation. *Development* **135**, 2521-2529.

Montalbano, M., Georgiadis, J., Masterson, A. L., McGuire, J. T., Prajapati, J., Shirafkan, A., Rastellini, C. and Cicalese, L. (2017). Biology and function of glypican-3 as a candidate for early cancerous transformation of hepatocytes in hepatocellular carcinoma (Review). *Oncol. Rep.* **37**, 1291-1300.

Montero, J.-A. and Heisenberg, C.-P. (2004). Gastrulation dynamics: cells move into focus. *Trends Cell Biol.* **14**, 620-627.

Nair, S. and Schilling, T. F. (2008). Chemokine signaling controls endodermal migration during zebrafish gastrulation. *Science* **322**, 89-92.

Ober, E. A., Field, H. A. and Stainier, D. Y. R. (2003). From endoderm formation to liver and pancreas development in zebrafish. *Mech. Dev.* **120**, 5-18.

Odenthal, J. and Nüsslein-Volhard, C. (1998). fork head domain genes in zebrafish. *Dev. Genes Evol.* **208**, 245-258.

Ohkawara, B., Yamamoto, T. S., Tada, M. and Ueno, N. (2003). Role of glypican 4 in the regulation of convergent extension movements during gastrulation in Xenopus laevis. *Development* **130**, 2129-2138.

Parsons, M. J., Pollard, S. M., Saude, L., Feldman, B., Coutinho, P., Hirst, E. M. and Stemple, D. L. (2002). Zebrafish mutants identify an essential role for laminins in notochord formation. *Development* **129**, 3137-3146.

Pézeron, G., Mourrain, P., Courty, S., Ghislain, J., Becker, T. S., Rosa, F. M. and David, N. B. (2008). Live analysis of endodermal layer formation identifies random walk as a novel gastrulation movement. *Curr. Biol.* **18**, 276-281.

Poulain, F. E. and Yost, H. J. (2015). Heparan sulfate proteoglycans: a sugar code for vertebrate development? *Development* **142**, 3456-3467.

Robu, M. E., Larson, J. D., Nasevicius, A., Beiraghi, S., Brenner, C., Farber, S. A. and Ekker, S. C. (2007). p53 activation by knockdown technologies. *PLoS Genet.* **3**, e78.

Roszko, I., Sawada, A. and Solnica-Krezel, L. (2009). Regulation of convergence and extension movements during vertebrate gastrulation by the Wnt/PCP pathway. *Semin. Cell Dev. Biol.* **20**, 986-997.

Rozario, T. and DeSimone, D. W. (2010). The extracellular matrix in development and morphogenesis: a dynamic view. *Dev. Biol.* **341**, 126-140.

Sepich, D. S., Usmani, M., Pawlicki, S. and Solnica-Krezel, L. (2011). Wnt/PCP signaling controls intracellular position of MTOCs during gastrulation convergence and extension movements. *Development* **138**, 543-552.

Sisson, B. E., Dale, R. M., Mui, S. R., Topczewska, J. M. and Topczewski, J. (2015). A role of glypican4 and wnt5b in chondrocyte stacking underlying craniofacial cartilage morphogenesis. *Mech. Dev.* **138**, 279-290.

Solnica-Krezel, L. and Sepich, D. S. (2012). Gastrulation: making and shaping germ layers. *Annu. Rev. Cell Dev. Biol.* **28**, 687-717.

Song, H. H. and Filmus, J. (2002). The role of glypicans in mammalian development. *Biochim. Biophys. Acta* **1573**, 241-246.

Srinivasan, S., Wang, F., Glavas, S., Ott, A., Hofmann, F., Aktories, K., Kalman, D. and Bourne, H. R. (2003). Rac and Cdc42 play distinct roles in regulating PI(3,4,5)P3 and polarity during neutrophil chemotaxis. *J. Cell Biol.* **160**, 375-385.

Stafford, D., White, R. J., Kinkel, M. D., Linville, A., Schilling, T. F. and Prince, V. E. (2006). Retinoids signal directly to zebrafish endoderm to specify insulin-expressing beta-cells. *Development* **133**, 949-956.

Strate, I., Tessadori, F. and Bakkers, J. (2015). Glypican4 promotes cardiac specification and differentiation by attenuating canonical Wnt and Bmp signaling. *Development* **142**, 1767-1776.

Theocharis, A. D. and Karamanos, N. K. (2017). Proteoglycans remodeling in cancer: underlying molecular mechanisms. *Matrix Biol.* (in press).

Thisse, C. and Thisse, B. (2008). High-resolution in situ hybridization to whole-mount zebrafish embryos. *Nat. Protoc.* **3**, 59-69.

Topczewski, J., Sepich, D. S., Myers, D. C., Walker, C., Amores, A., Lele, Z., Hammerschmidt, M., Postlethwait, J. and Solnica-Krezel, L. (2001). The zebrafish glypican knypek controls cell polarity during gastrulation movements of convergent extension. *Dev. Cell* **1**, 251-264.

Trichas, G., Smith, A. M., White, N., Wilkins, V., Watanabe, T., Moore, A., Joyce, B., Sugnaseelan, J., Rodriguez, T. A., Kay, D. et al. (2012). Multi-cellular rosettes in the mouse visceral endoderm facilitate the ordered migration of anterior visceral endoderm cells. *PLoS Biol.* **10**, e1001256.

Trinh, L. A. and Stainier, D. Y. R. (2004). Fibronectin regulates epithelial organization during myocardial migration in zebrafish. *Dev. Cell* **6**, 371-382.

Turunen, S. P., Tatti-Bugaeva, O. and Lehti, K. (2017). Membrane-type matrix metalloproteases as diverse effectors of cancer progression. *Biochim. Biophys. Acta* **1864**, 1974-1988.

Venero Galanternik, M., Lush, M. E. and Piotrowski, T. (2016). Glypican4 modulates lateral line collective cell migration non cell-autonomously. *Dev. Biol.* **419**, 321-335.

Villefranc, J. A., Amigo, J. and Lawson, N. D. (2007). Gateway compatible vectors for analysis of gene function in the zebrafish. *Dev. Dyn.* **236**, 3077-3087.

Warga, R. M. and Nüsslein-Volhard, C. (1999). Origin and development of the zebrafish endoderm. *Development* **126**, 827-838.

Woo, S., Housley, M. P., Weiner, O. D. and Stainier, D. Y. R. (2012). Nodal signaling regulates endodermal cell motility and actin dynamics via Rac1 and Prex1. *J. Cell Biol.* **198**, 941-952.

Xu, H., Echemendia, N., Chen, S. and Lin, F. (2011). Identification and expression patterns of members of the protease-activated receptor (PAR) gene family during zebrafish development. *Dev. Dyn.* **240**, 278-287.

Ye, D. and Lin, F. (2013). S1pr2/Galpha13 signaling controls myocardial migration by regulating endoderm convergence. *Development* **140**, 789-799.

Ye, D., Xie, H., Hu, B. and Lin, F. (2015). Endoderm convergence controls subduction of the myocardial precursors during heart-tube formation. *Development* **142**, 2928-2940.

Young, T., Poobalan, Y., Tan, E. K., Tao, S., Ong, S., Wehner, P., Schwenty-Lara, J., Lim, C. Y., Sadasivam, A., Lovatt, M. et al. (2014). The PDZ domain protein Mcc is a novel effector of non-canonical Wnt signaling during convergence and extension in zebrafish. *Development* **141**, 3505-3516.

Zinkevich, N. S., Bosenko, D. V., Link, B. A. and Semina, E. V. (2006). laminin alpha 1 gene is essential for normal lens development in zebrafish. *BMC Dev. Biol.* **6**, 13.
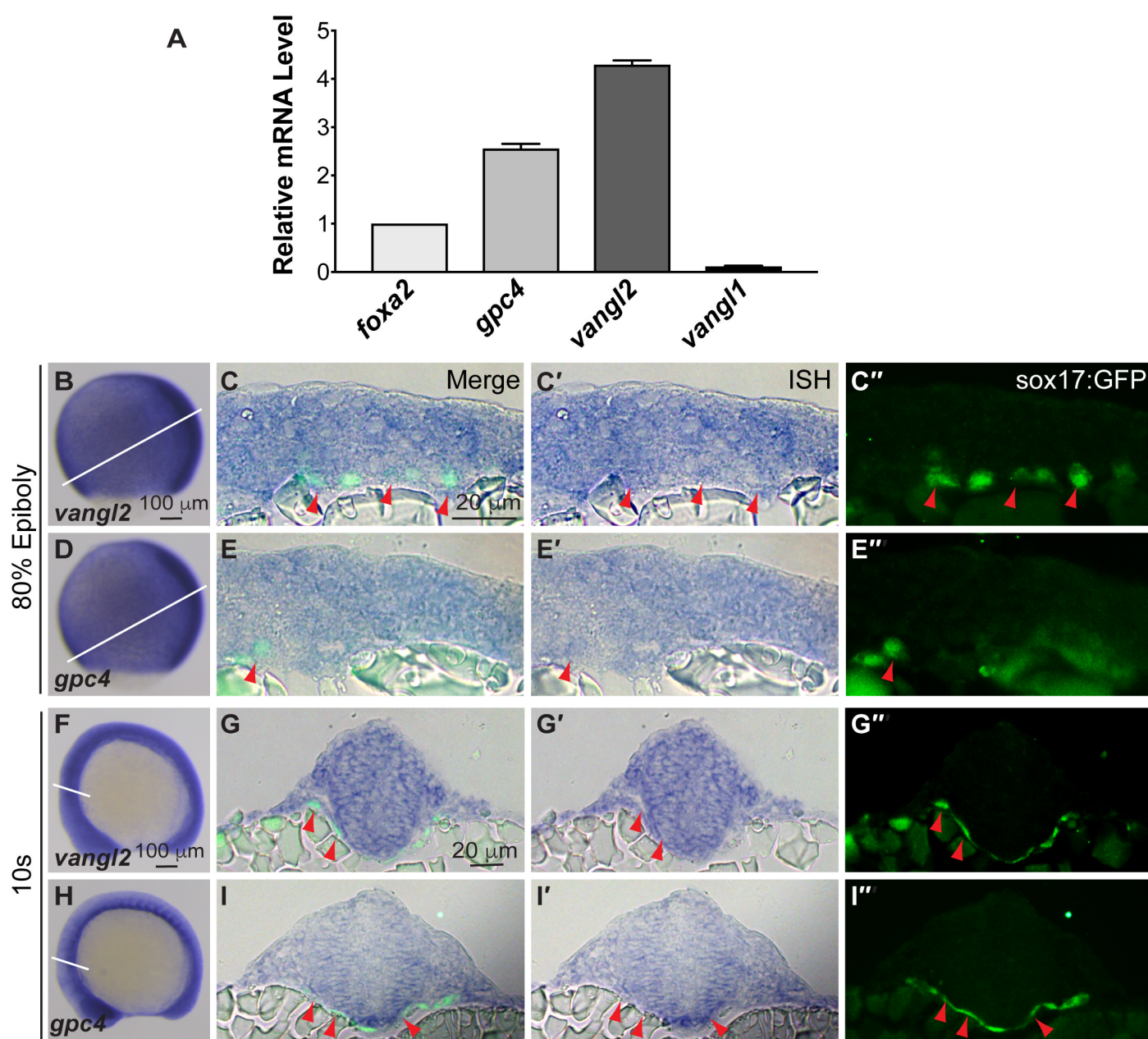
**Figure S1. The expression of *gpc4* and *vangl2* during gastrulation and early segmentation**.

(**A**) Expression of *gpc4*, *vangl2* and *vangl1* relative to that of *foxa2,* and endoderm marker, as determined by qRT-PCR, in GFP⁺ cells sorted from *Tg(sox17:EGFP)* embryos at 18s. Bars represent the mean±s.e.m. (**B-I″**) The expression of *gpc4* and *vangl2* transcripts in *Tg(sox17:EGFP)* embryos at 80%E and 10 s, as detected by WISH. (B, D, F, H) Images of the whole embryo. White lines indicate the cross-sectional plane. (C-C″, E-E″, G-G″, I-I″) Transverse sections of the embryos. (C, E, G, I) Overlays of anti-GFP immunofluorescence staining (*sox17:EGFP* panels) and ISH for *vangl2* and *gpc4* (ISH panels), in endodermal cells (red arrowheads).
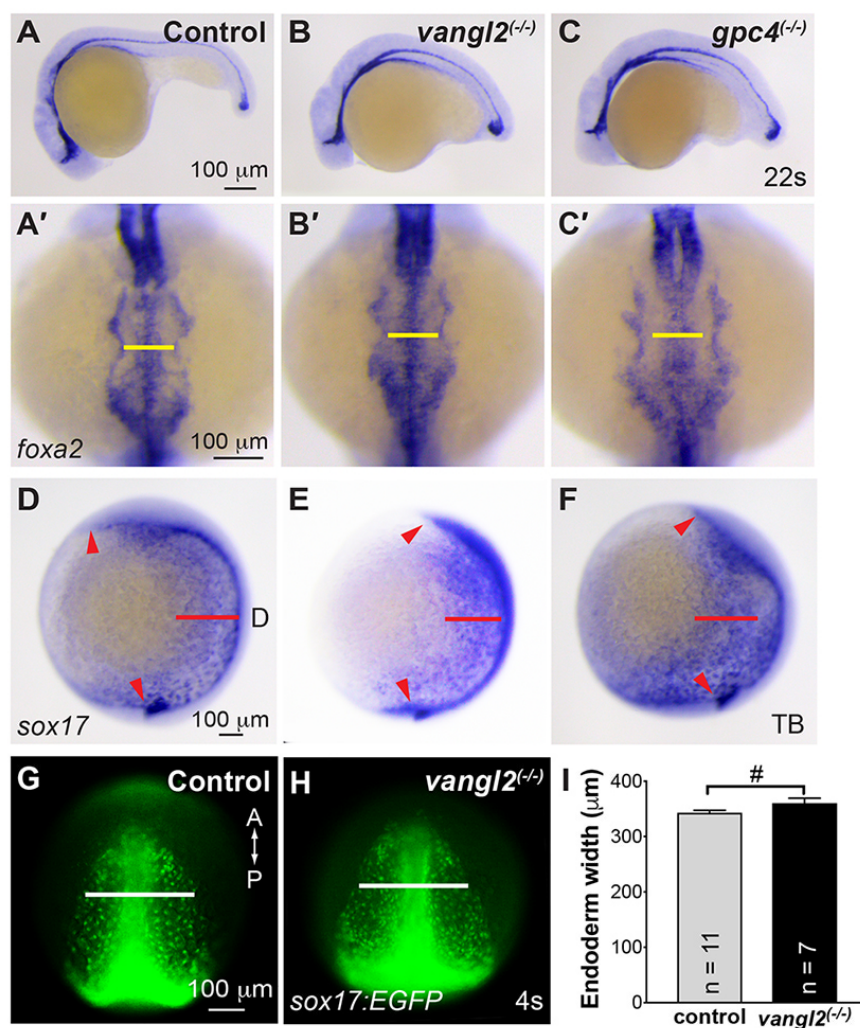
Figure S2. Gpc4, but not Vangl2, is required for convergence of the anterior endoderm.

(**A-F**) Expression of *foxa2* (A-C′) and *sox17* (D-F) in the indicated embryos, as detected by WISH. Lateral (A-C, D-F) and anterior-dorsal (A′-C′) views. Yellow lines of equivalent length indicate width of the anterior endodermal sheets. Red lines of equivalent length indicate the distance between the lateral-most endodermal cells and the dorsal site of embryo. Red arrowheads indicate the end of anterior and posterior body axes. D, dorsal. (**G,H**) Epifluorescence images of anterior endoderm in control, *vangl2* mutant *Tg(sox17:EGFP)* embryos at 4s. Anterior-dorsal view. White lines of equivalent length indicate width of the anterior endodermal sheets. A, anterior; P, posterior. (**I**) Quantification of endoderm width in each group of embryos shown in (G,H). Number of embryos for each group is indicated. Bars represent the mean±s.e.m. #, p>0.05; student's *t*-test.
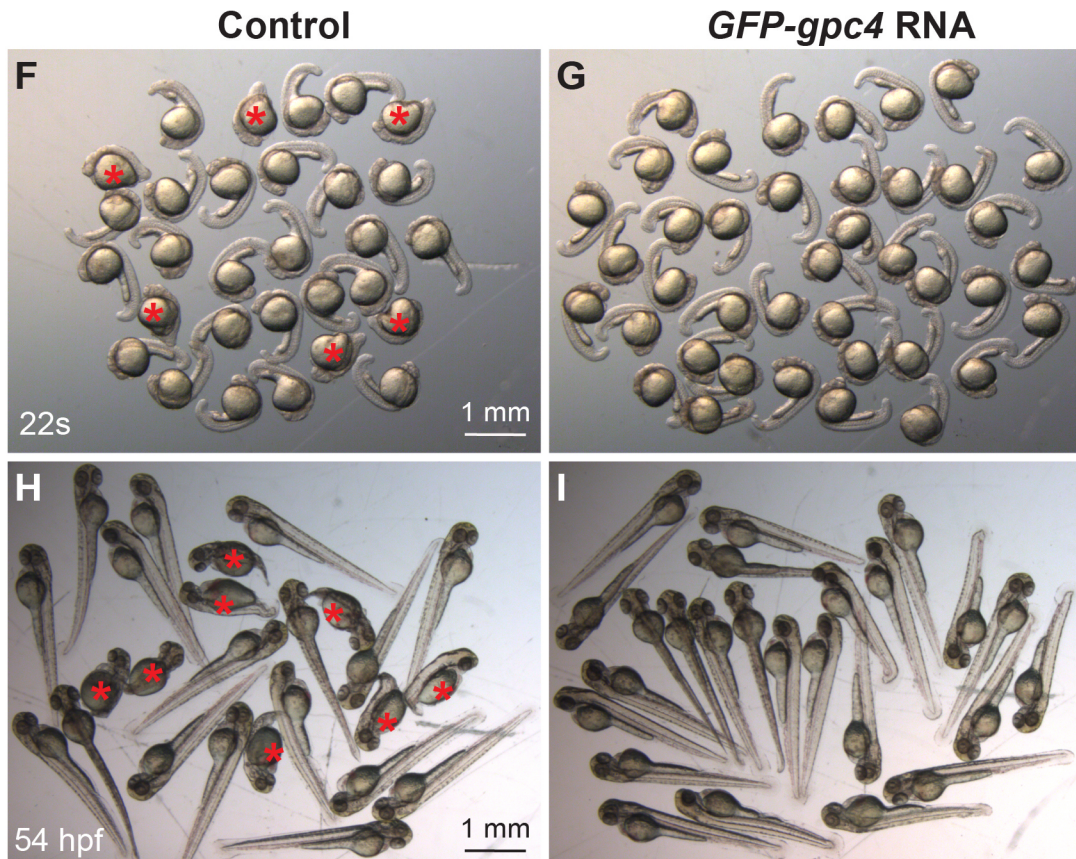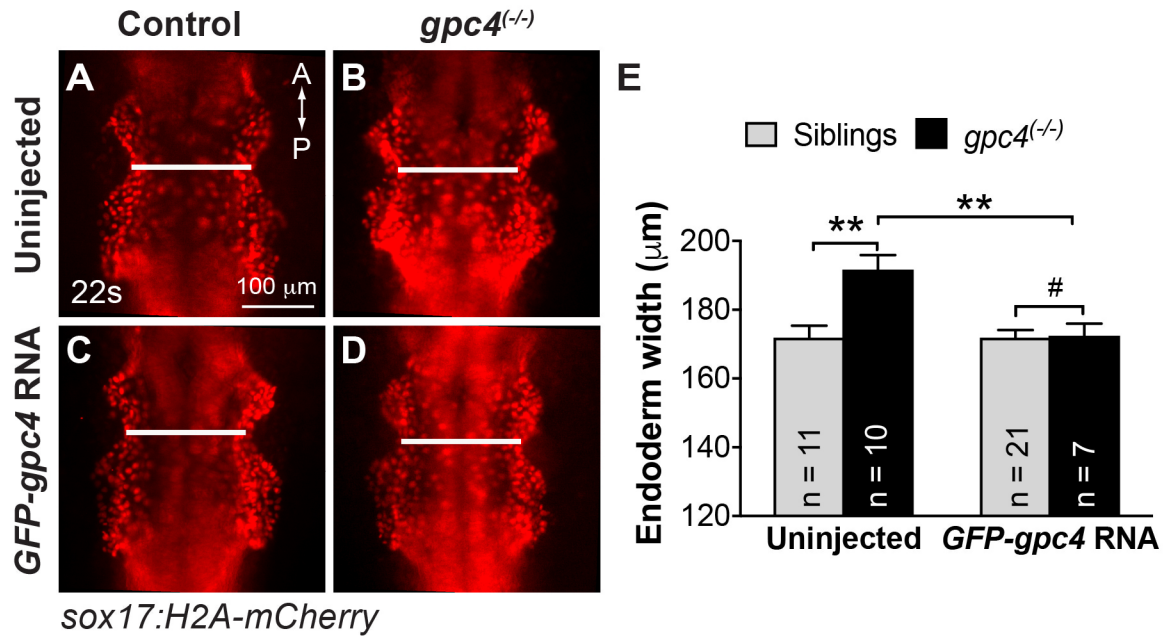
sox17:H2A-mCherry

Figure S3. Overexpression of GFP-Gpc4 rescues defects in length of body axis and convergence of anterior endoderm in *gpc4* mutant embryos.

(**A-D**) Representative images of indicated *Tg(sox17:H2A-mCherry)* embryos injected with or without *GPF-gpc4* RNA at 22s. Anterior-dorsal view; white lines of equivalent length indicate width of the anterior endodermal sheets. A, anterior; P, posterior. (**E**) Quantification of the width of the anterior endodermal sheet in each group of embryos shown in (A-D). Data represent mean±s.e.m. The number of embryos is indicated. #, P>0.05; **, P<0.01, student's t-test.(**F-I**) Bright-field images of groups of embryos derived from crosses of *gpc4*$^{(+/-)}$ injected with or without *GPF-gpc4* RNA at 22s and 54 hpf. Red asterisks indicate *gpc4* homozygous embryos with a short anterior-posterior body axis.
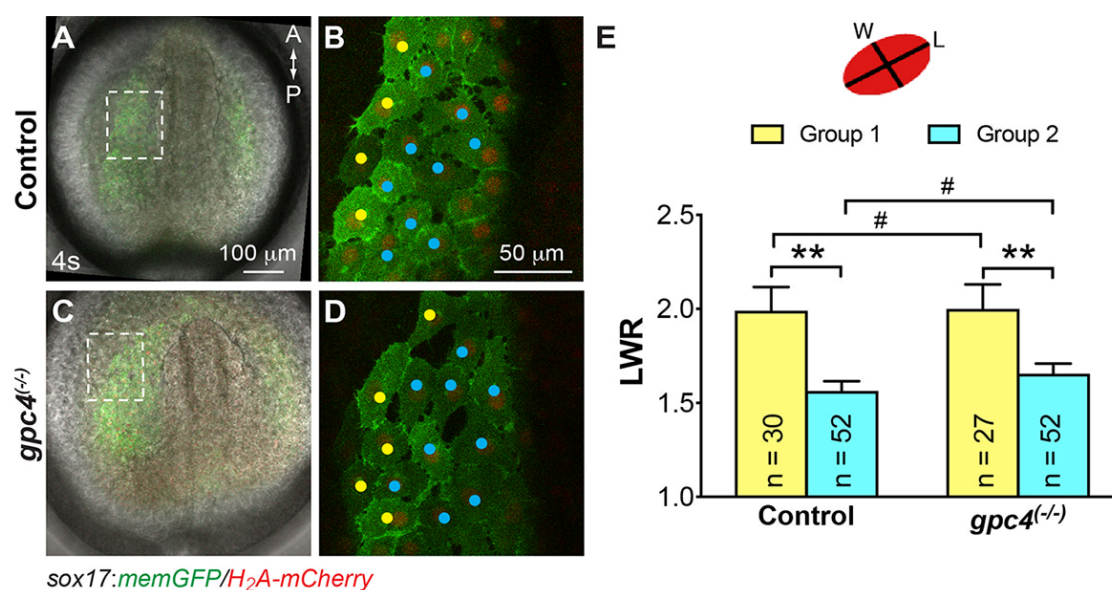
Figure S4. Morphology of anterior endodermal cells is not affected in *gpc4* mutants. (**A,C**) Overlay of bright-field and epifluorescence images of *Tg(sox17:memGFP/H₂A-mcherry)* embryos at 4s. Dashed boxes are regions in which cells were imaged for analysis of shape. (**B, D**) Confocal images of the endoderm at the region indicated in the dashed boxes in A, C. Endodermal cells at the lateral region and near the dorsal midline are labeled with yellow and cyan dots, respectively. A, anterior; P, posterior. (**E**) Schematic representation of the method used to measure cell shape (LWR, length-to-width ratio). Quantification of LWR of endodermal cells in seven control and six *gpc4* mutant embryos. Bars represent the mean±s.e.m. The number of cells analyzed is indicated. #, p>0.05; **, P<0.01, student's t-test.
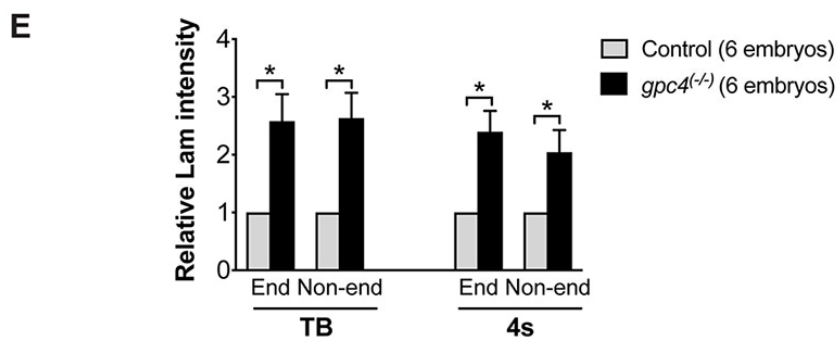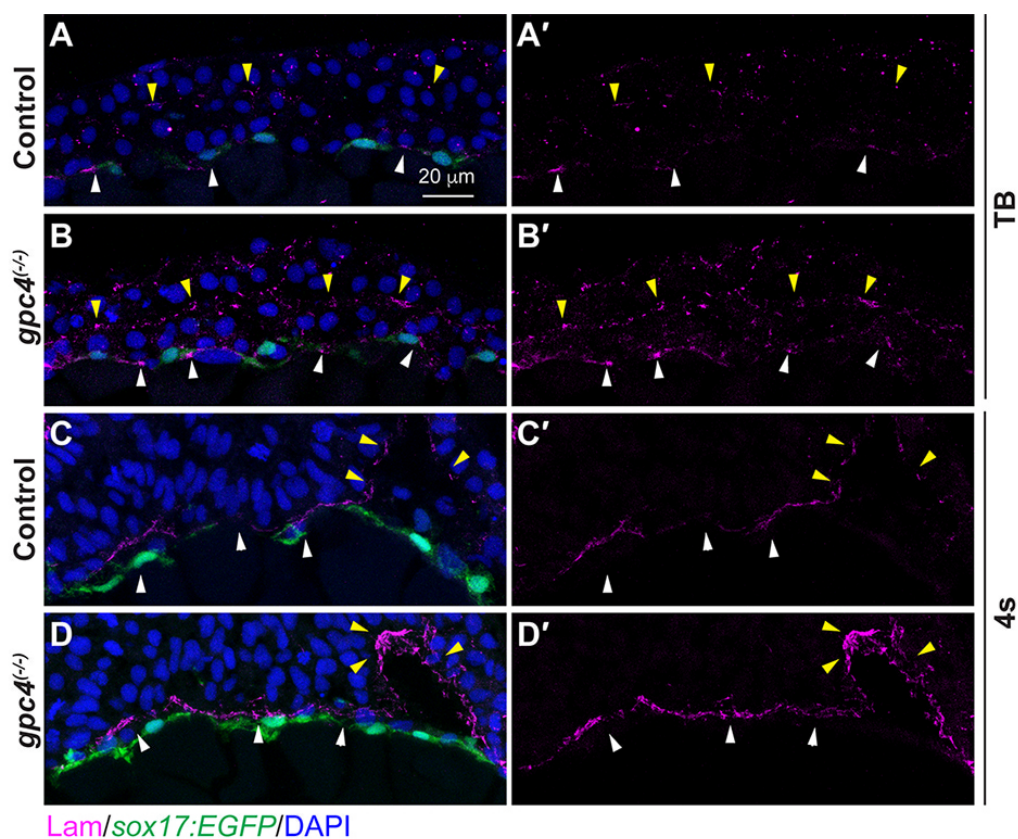
Figure S5. Lam deposition is increased in *gpc4* mutant embryos.

Transverse cryosections from *Tg(sox17:EGFP)* control and *gpc4* mutant embryos immunostained for Lam (magenta) and nuclei (DAPI, blue). (**A-D′**) Confocal z-stack images of embryos at tailbud (TB) (A-B′) and 4-somite (4s) (C-D′) stages. Lam assembly between the ectoderm and mesoderm (yellow arrowheads) and around the endodermal layer (white arrowheads). (**E**) Relative Lam intensity in non-endodermal (Non-end) tissue and around the endodermal layer (End) in control and *gpc4* mutant embryos at TB and 4s. The number of embryo analyzed is shown in the graph. Bars represent the mean±s.e.m. *, $P<0.05$, student's t-test.
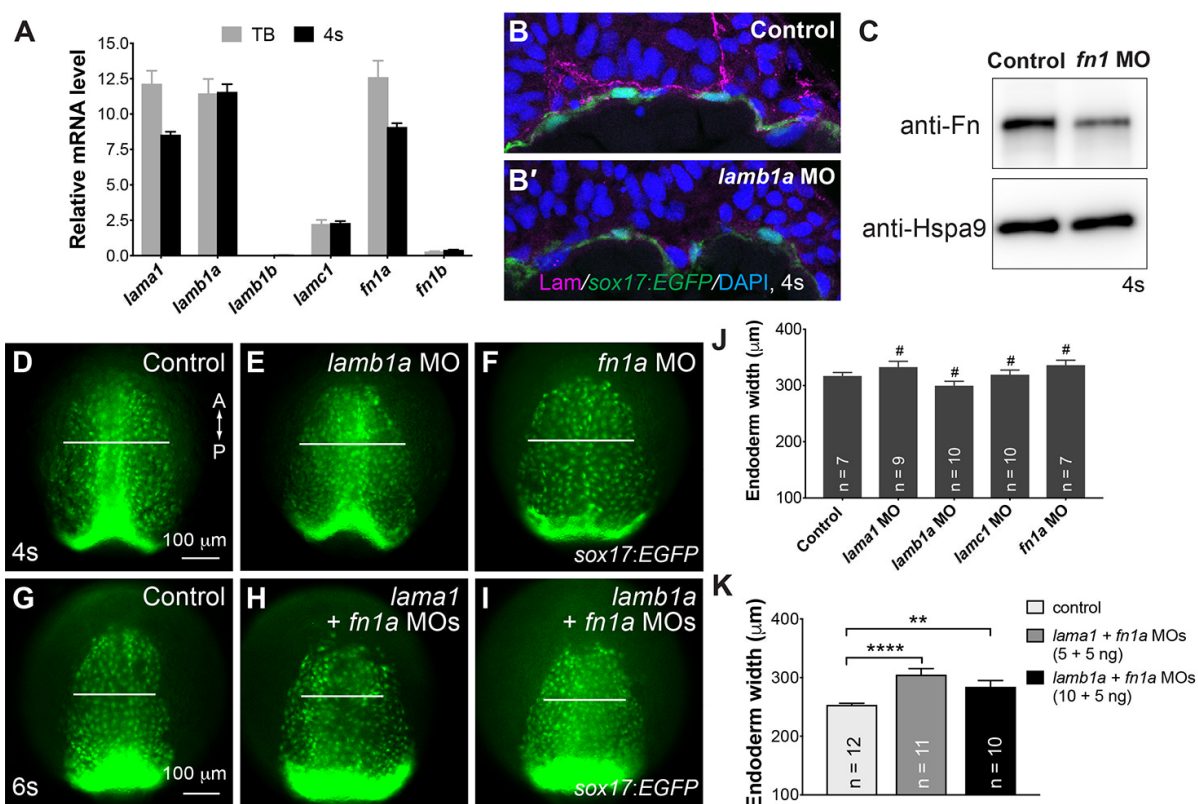
Figure S6. Effects of suppressing Fn or/and Lam expression on endoderm C&E.

(**A**) Expression of *lam1* (*a1, b1a, b1b, c1*) and *fn* (*1a and 1b*) relative to that of the housekeeping gene *eukaryotic translation elongation factor 1 alpha 1a (eef1a)* in WT embryos at TB and 4s, as determined by qRT-PCR. (**B-B′**) Confocal z-stack images of transverse cryosections immunostained for Lam (magenta) and nuclei (DAPI, blue) from the indicated embryos. (**C**) Western blot showing expression levels of Fn and Hspa9 (internal control) in embryos indicated. (**D-I**) Epifluorescence still images of the anterior endodermal sheet in embryos indicated. Anterior-dorsal view. A, anterior; P, posterior. White lines of equivalent length indicate width of anterior endodermal sheet of the embryos at the same stage. (**J,K**) Average width of anterior endoderm. (J) Embryos injected with the indicated MO (10 ng), shown in (D-F). (K) Embryos treated as indicated and shown in (G-I). Number of embryos analyzed is indicated for each group. #, p>0.05, **, p<0.01, ****, p<0.0001, student's t-test.
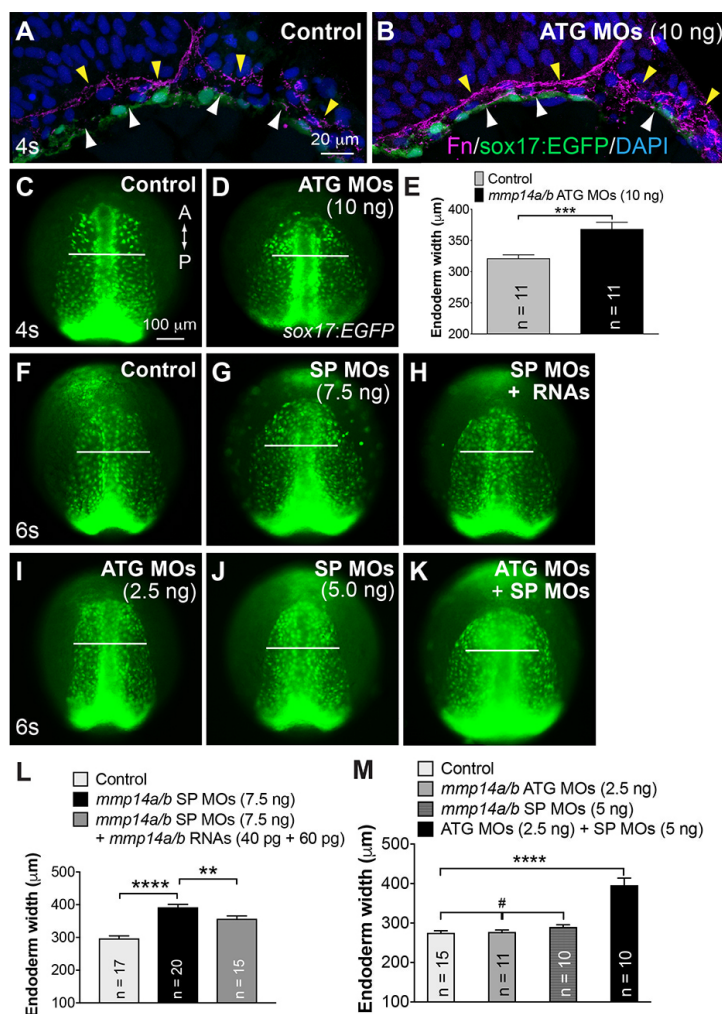
Figure S7. Mmp14a/b are required for C&E movements of the anterior endodermal cells.
(**A-B**) Confocal z-stack images of transverse cryosections from *Tg(sox17:EGFP)* control embryos and
embryos injected with *mmp14a/b* ATG MOs (10ng, suppression of translation) immunostained for Fn
(magenta) and nuclei (DAPI, blue). Fn assembly at mes/end (white arrowheads) and ect/mes (yellow
arrowheads) boundaries. (**C-M**) Embryos injected with indicated MOs targeting *mmp14a/b* (ATG MOs
target the translation; SP MOs target the splicing). (C-D, F-K) Epifluorescence still images of the anterior
region of the endodermal sheet in the indicated embryos. Anterior-dorsal view. A, anterior; P, posterior.
White lines of equivalent length indicate the width of anterior endodermal sheets of the embryos at the
same stage. (E) Average endodermal width at the anterior region of embryos shown in (C,D). (L)
Average width of anterior endoderm in embryos shown in (F-H). (M) Average width of anterior
endoderm in embryos shown in (I-K). The number of embryos analyzed in each group is indicated. **,
p<0.01; ***, p<0.001; ****, p<0.0001; #, p>0.05, student's *t*-test.
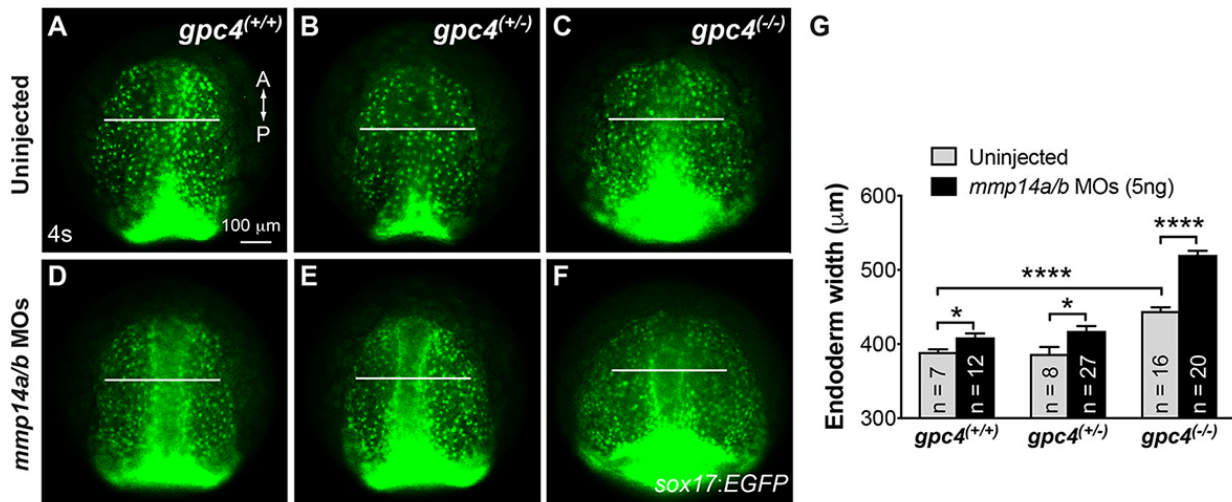
Figure S8. Mmp14a/b and Gpc4 act synergistically in regulating endodermal migration.
(**A-F**) Epifluorescence still images of the anterior endoderm at 4s in embryos derived from crosses of
gpc4/Tg(sox17:EGFP) heterozygous zebrafish injected with or without a subdose of *mmp14a/b* ATG
MOs (5 ng). White lines of equivalent length indicate the width of anterior endodermal sheets. A,
anterior; P, posterior. (**G**) Average endoderm width in the anterior region. Numbers of embryos analyzed
are indicated for each group. *, p<0.05; ****, p<0.0001; student's t-test.
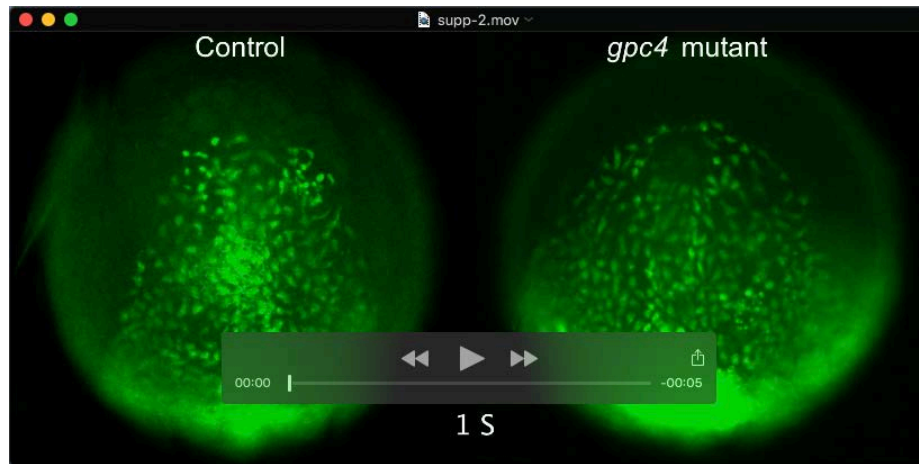
Movie 1. Gpc4 is required for efficient endoderm C&E during early segmentation.

Time-lapse experiments were performed on *Tg(sox17:EGFP)* control or *gpc4* mutant embryos from 1-6s, using an epifluorescence microscope (DMI 6000, Leica) with a 5x/NA 0.15 objective. Images were acquired at 5-min intervals and movie plays at 5 frames/sec.
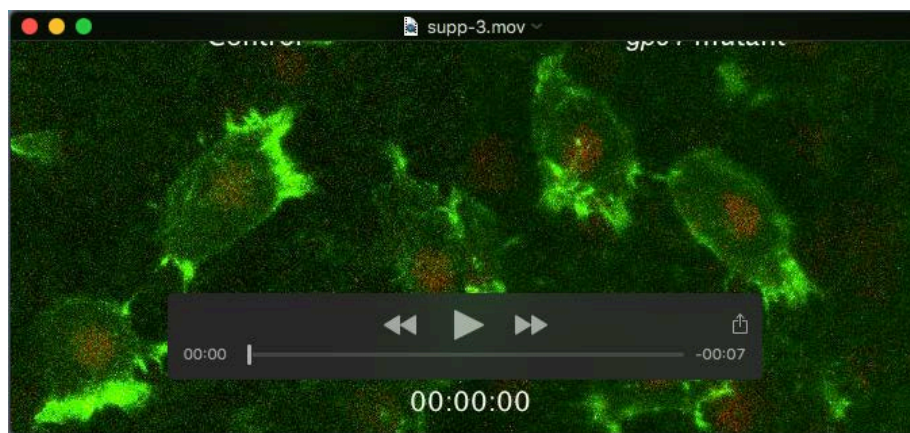

Movie 2. Polarized actin-rich protrusions of migrating endodermal cells in control and *gpc4* mutant embryos.

Confocal time-lapse experiments were performed on *Tg(sox17:GFP-UTRN)* control or *gpc4* mutant embryos at TB, using a Ziess LSM700 confocal microscope with a LD C-Apo 40×/NA 1.1 water objective. Images were acquired at 10-sec intervals and movie plays at 5 frames/sec.
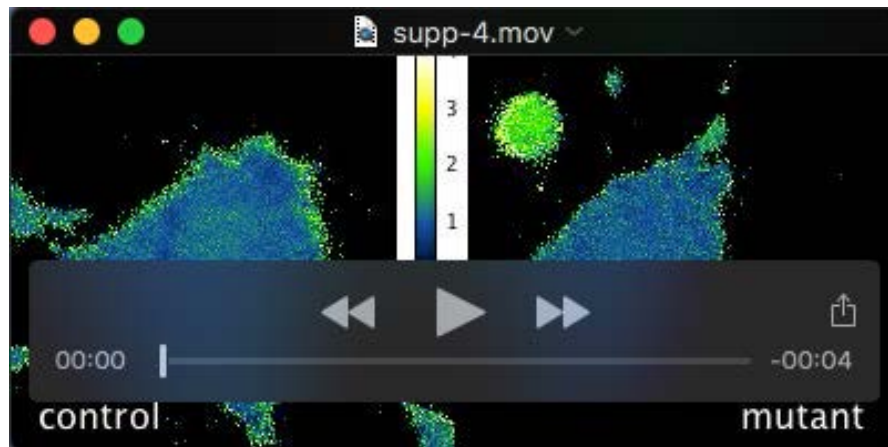
**Movie 3. Rac1 activity in migrating endodermal cells in control and *gpc4* mutant embryos.**
Representative time-lapse movies of anterior endoderm in control (left panel) or *gpc4* mutant (right panel)
host embryo transplanted with *sox32,* PDB-GFP-expressing and rhodamine-labeled control (left panel) or
gpc4 mutant (right panel) cells. Images were acquired at 10-sec intervals using a Ziess LSM700 confocal
microscope with a LD C-Apo 40×/NA 1.1 water objective and movie plays at 5 frames/sec.
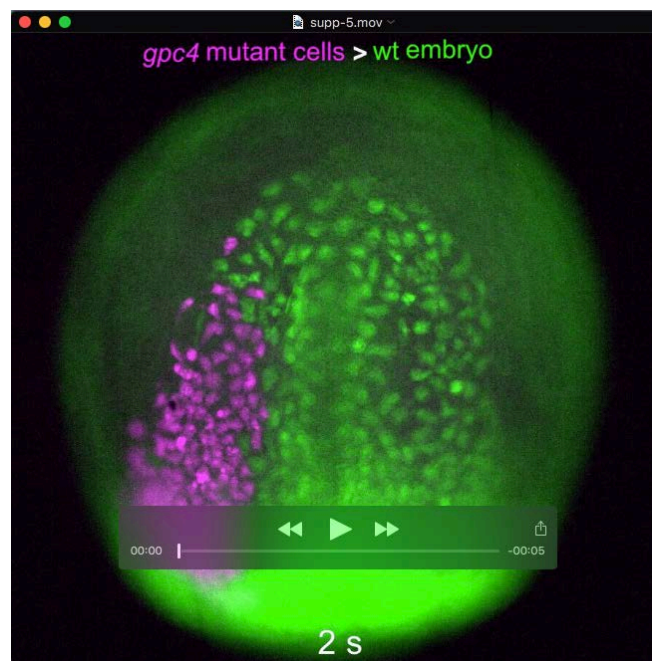
**Movie 4. C&E of *gpc4*-deficient donor cells in wild-type host embryo.**
Representative time-lapse movie of anterior endoderm of a *Tg(sox17:EGFP)* embryo transplanted with
sox32-expressing, rhodamine-labeled *gpc4*-deficient cells (magenta), from 2-5s. Images were captured at
5-min intervals using an epifluorescence microscope (DMI 6000, Leica) with a 5x/NA 0.15 objective.
The movie plays at 5 frames/sec.
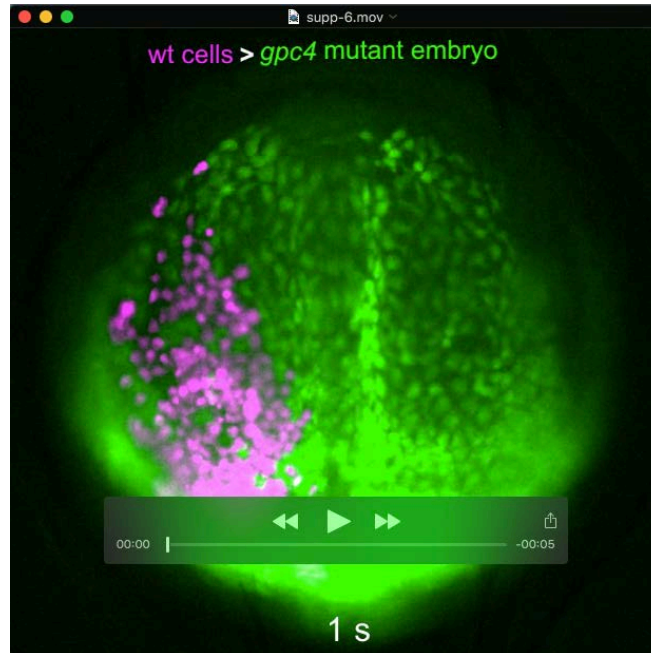
Movie 5. C&E of wild-type donor cells in *gpc4* mutant.

Representative time-lapse movie of anterior endoderm of a *Tg(sox17:EGFP) gpc4* mutant transplanted with *sox32*-expressing, rhodamine-labeled wild-type cells (magenta), from 1-5s. Images were captured at 5-min intervals using an epifluorescence microscope (DMI 6000, Leica) with a 5x/NA 0.15 objective. The movie plays at 5 frames/sec.
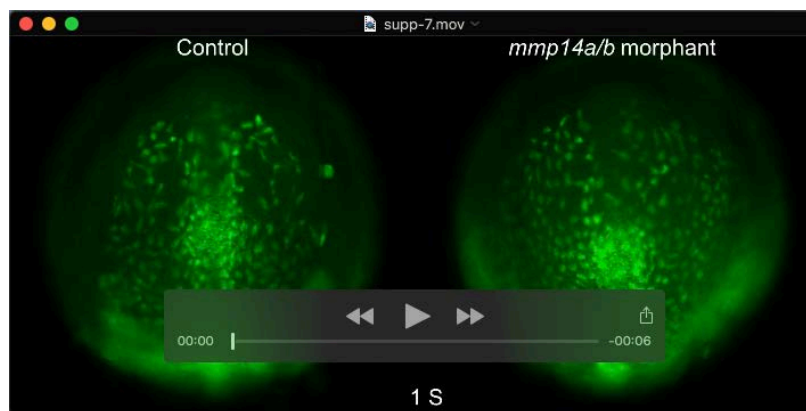
Movie 6. Mmp14a/b is required for efficient endoderm C&E during early segmentation.

Time-lapse experiments were performed on control or *mmp14a/b* MO-injected *Tg(sox17:EGFP)* embryos from 1-6s, using an epifluorescence microscope (DMI 6000, Leica) with a 5x/NA 0.15 objective. Images were acquired at 5-min intervals. The movie plays at 5 frames/sec.
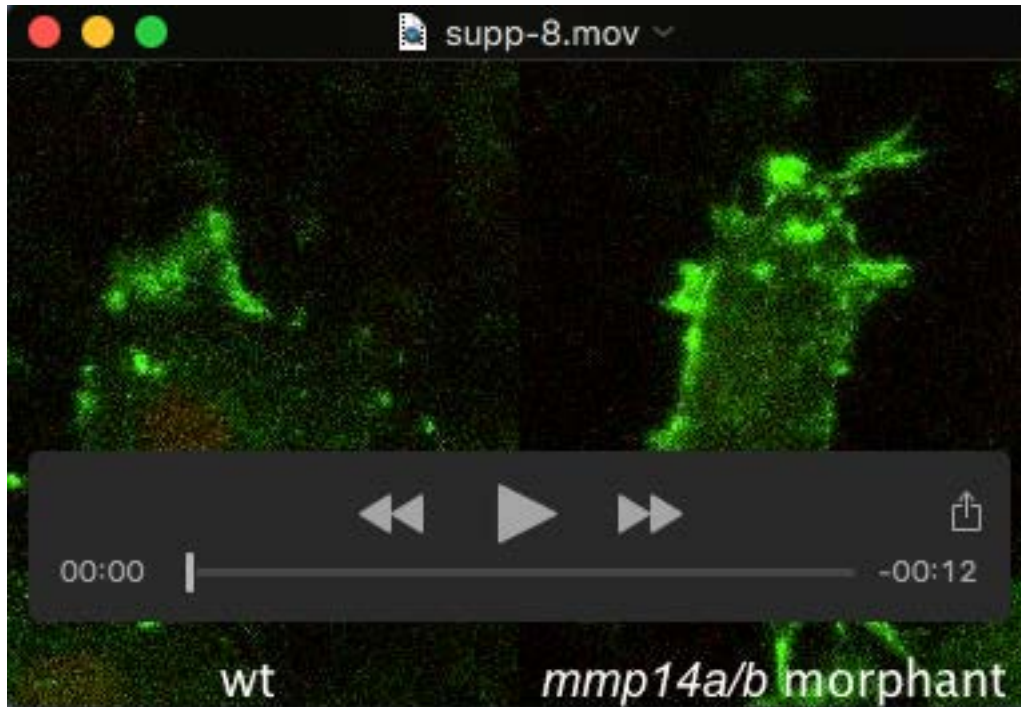
Movie 7. Polarized actin-rich protrusions of migrating endodermal cells in control and *mmp14a/b* MO-injected embryos.

Confocal time-lapse experiments were performed on *Tg(sox17:GFP-UTRN)* control or *mmp14a/b* MO-injected embryos at TB, using a Zeiss LSM700 confocal microscope with a LD C-Apo 40×/NA 1.1 water objective. Images were acquired at 10-sec intervals, and movie plays at 5 frames/sec.

Supplemental table 1: The sequences of primers used for qRT-PCR of the indicated genes

Genes	Forward sequence (5'-3')	Reverse sequence (5'-3')
vangl1	AACTCACCACTATAACATGGGACAA	CACTTCCAGCACCATCCACA
vangl2	TTCCCAAATCCATCCTGTCCAA	GGTCCATCTCAGCCTCCTCGTAG
gpc4	CAGCTCAAACCCTTCGGAGAC	CGCTACAGTACGGGCAGTATAACAT
foxa2	CAGACTGGAGCACTTACTACGG	AGGACATGTTCATGGTGTTAGC
eef1a1a	GAGAAGTTCGAGAAGGAAGC	CGTAGTATTTGCTGGTCTCG
fn1a	GTGTATGCCGAAAGGAACG	CCCGGTAGGAACGAGAATT
fn1b	GTTTAGCCATCCACGAAAGT	AGTCCCATATCATGTTATCCTTT
lama1	CTGCCCCTGGGACCCTGTTA	TCCGCCACCGTCTGGTTGTA
lamb1a	CGCACCAAGTAACCAGCCACA	GCCGAACGCTCGATCACCA
lamb1b	GTGACAACCTTCGCTCCCA	GCCAGGTCCTCCCATAATCT
lamc1	TAGCGACATCTCGCCACTC	ACTTGCACCTTCCTCCCAC
mmp14a	GTGTTTCTGGTGCAGAGCG	CCGAGATAGCGGAGTTGATAG
mmp14b	CTGGAGCGGGTTTACGAGG	CATGGCAGCAATGGCAGAG